THE GEODYNAMIC SETTING OF THE NAIN OPHIOLITES, CENTRAL IRAN: EVIDENCE FROM CHROMIAN SPINELS IN THE CHROMITITES AND ASSOCIATED ROCKS

Javad Mehdipour Ghazi*,✉, Mohssen Moazzen, Mohammad Rahghoshay*** and **Hadi Shafaii Moghadam*****

* *Department of Geology, Shahid Beheshti University, Tehran, Iran.*
** *Department of Geology, University of Tabriz, Iran.*
*** *School of Earth Sciences, University of Damghan, Iran.*
✉ *Correspondig author, e-mail: jm.ghazi@yahoo.com*

Keywords: *Nain ophiolites, Cr-spinel, chromitite, boninitic melt, inter-oceanic arc, oceanic back-arc basin. Iran.*

ABSTRACT

In central Iran, to the northwest of the Central Iranian micro-continental (CIM) block, the coloured mélange is characterized by widespread ophiolite blocks. In the Nain area, these ophiolite blocks, known as Nain ophiolites, are mainly composed of mantle peridotites. Based on field and petrographic observations and on the chemistry of Cr-spinels, two types of chromitites have been recognized in the Nain ophiolites. The first type occurs as chromitite patches within the harzburgites. The Cr number [$Cr^{\#}$ = 100*Cr/(Cr+Al)] of the Cr-spinels varies between 58 and 63 in chromitite patches and 39-40 in harzburgites. Calculated amount of Al_2O_3 and ratio of FeO/MgO in the parental melts of the chromitite patches indicate a boninitic melts for the source magmas of the Cr-spinels. The REE patterns for the studied harzburgites and lherzolites are similar to those from abyssal peridotites. These characteristics suggest a back-arc basin setting for the generation of the chromitite patches as well as of the harzburgites and lherzolites from the Nain ophiolites. The second type of chromitites occurs as lenses (chromitite pods) in dunites. The Cr number of Cr-spinels of these chromitites varies between 69 and 73. The Cr-spinels of these chromitites also show a boninitic nature for the parental melts. These characteristics of chromitite lenses show that they were generated at an arc setting. Therefore, intra-oceanic subduction in the Nain basin in Early Cretaceous can be proposed on the basis of these data on the origin of the chromitite lenses. Intra-oceanic rifting in a back-arc setting generated an oceanic back-arc basin in the Nain area in Late Cretaceous., The chromitite patches and the studied harzburgites and lherzolites were likely formed in the mantle beneath the back-arc basin. On the whole, the field and petrographic observations as well as the degree of partial melting, calculated on the basis of the $Cr^{\#}$, suggest that the genesis of these rocks can be explained according to a mixed open-channel cumulate/rock-reaction model.

INTRODUCTION

Ophiolites are considered to be important tools for understanding the tectonic and magmatic processes responsible for the formation of oceanic lithosphere. The lithological and chemical signatures of their mantle section can provide further insights into the tectonic setting where the ophiolitic complexes formed.

Cr-spinel is an important petrogenetic indicator in ultramafic/mafic rocks. It is recognized as a sensitive mineral for deducing the conditions during magma crystallization (e.g., Orberger et al., 1995; Kamenetsky et al., 2001). The major factors controlling the composition of Cr-spinel are: (i) composition of the parental melt, (ii) composition of minerals crystallizing along with Cr-spinel, (iii) the congruent/incongruent melting behaviour of the mantle, (iv) nature of crystallisation (equilibrium or fractional crystallisation) and (v) physico-chemical parameters (temperature, pressure, fO_2; e.g., Dick and Bullen, 1984; Dick and Kelemen, 1991).

Based on field relationships, petrographic studies, chemistry of Cr-spinel in chromitites and whole rock chemistry of peridotites, this paper attempts to interpret the possible tectonic environment for the origin of chromitites and associated mantle rocks in the Nain ophiolites. A magmatic and geodynamic model for the formation of the Nain ophiolites is also proposed.

GEOLOGICAL SETTING

The Iranian ophiolites (Fig. 1) belong to the Tethyan ophiolite belt of the Middle East. They have been divided into four groups (Takin, 1972; Stöcklin, 1974; McCall, 1997):

1- ophiolites of Northern Iran, cropping out along the Alborz Range, and regarded as remnants of the Paleo-Tethys Ocean (e.g., Ruttner, 1993; Moazzen et al., 2010);

2 - ophiolites of the Zagros Suture Zone, including those of Neyriz and the Kermanshah, which are correlated to the Oman ophiolites obducted onto the Arabian continental block (e.g., Lanphere and Pamić, 1983);

3 - ophiolites of the Makran region, which are located south of the Sanandaj-Sirjan Zone, and include non-fragmented complexes such as Sorkhband and Rudan (McCall, 1997; Ghazi et al., 2004);

4 - ophiolites enclosed as tectonic blocks in the Late Cretaceous coloured mélange along the main boundaries of the Central Iranian Micro-continental (CIM) (=Lut) block. To group 4 belong also some ophiolites from the Makran region and from the Sanandaj-Sirjan Zone.

The Nain ophiolites belong to group 4, according to Ghazi et al. (2004). Like the other ophiolites of this group, also the Nain ophiolites are regarded to be derived from the Cretaceous oceanic lithosphere surrounding the CIM block, located south-east of the Eurasia continental plate. Paleomagnetic data indicate that during the Mesozoic the CIM moved northwards, and contemporaneously underwent a counterclockwise rotation of about 130° towards the southern rim of Eurasia (Schmidt and Soffel, 1983), leading to development of subduction zones where the oceanic lithosphere was deformed and metamorphosed. As a result of this geodynamic evolution, several main suture zones developed around the CIM block, all marked by ophiolite-bearing coloured mélanges. Despite the occurrence of ophiolites in

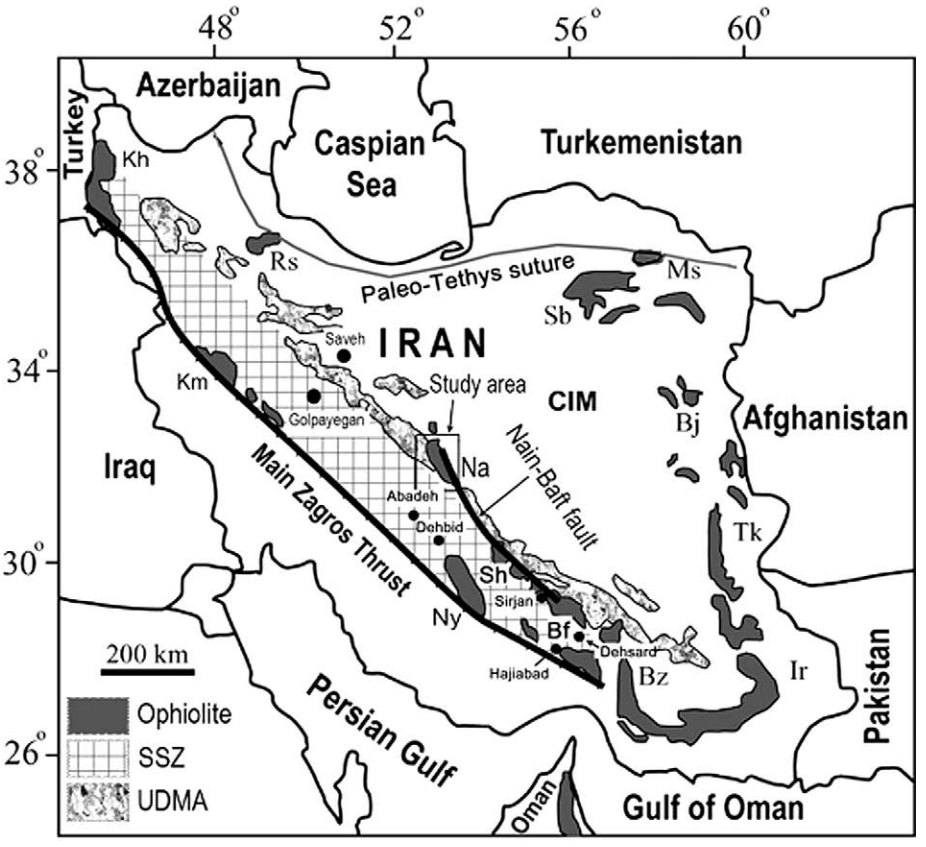

Fig. 1 - Sketch map of Iran showing locations of the major ophiolites, Sanandaj-Sirjan Zone (SSZ) and Urmia-Dokhtar magmatic arc (UDMA). Kh- Khoy; Kr- Kermanshah; Ny- Neyriz; Bz- Band-e-Zeyarat; Na- Nain; Bf- Baft; Sh- Shahr-Babak; Ir- Iranshahr; Tk- Tchehel Kureh; Ms- Mashad; Sb- Sabzevar; Rs- Rasht (Talesh ophiolite); Bj- Birjand (Modified after Emami et al., 1993).

the coloured mélanges as dismembered blocks, in the Nain, Sabzevar, Baft, Sistan and Makran areas all the components of a complete ophiolite sequence occur.

The Nain ophiolites crop out in an approximately 600 km^2 wide area, north of the town of Nain, along the Nain-Baft fault zone (Fig. 1). This fault represents a true suture zone running along the western side of the CIM, where several dismembered fragments of Neo-Tethyan ophiolites occur (Shojaat et al., 2003) as, for instance, those of Shahr-e-Babak, Dehshir, Balvard and Robat areas. The Nain-Baft suture zone is located northward of the Mesozoic magmatic arc of the active margin of the Central Iranian block, reported in literature also as Sanandaj-Sirjan Zone. The Sanandaj-Sirjan Zone is a narrow zone of highly deformed rocks dominated by Mesozoic rocks, while the Palaeozoic rocks are generally rare and restricted to the southeast.

Three $^{40}Ar/^{39}Ar$ ages of 101.2±0.9, 99.7±0.9, 99±1.2 Ma obtained on a hornblende gabbro indicate a late Albian age for the Nain ophiolites (Hassanipak and Ghazi, 2000). K-Ar ages, performed on amphibole grains from amphibolites and gabbros, reveal in turn a Middle to Late Cretaceous age plateau for the Nain-Baft ophiolitic belt (Shafaii Moghadam et al., 2007).

In addition, Rahmani et al. (2007) proposed for the sheeted dykes of the Nain ophiolites an origin related to a suprasbduction zone (SSZ).

In the available literature, the ophiolites from the Nain-Baft suture zone have been interpreted as (i) remnants of a narrow oceanic basin, like the Red Sea, located between the CIM block and the Sanandaj-Sirjan Zone (e.g., Berberian and King, 1981); (ii) as remnants of a Cretaceous arc basin related to Tethyan subduction (e.g., Desmons and Beccaluva, 1983) and (iii) as remnants of a Late Cretaceous back-arc basin (e.g., Agard et al., 2006; Ghazi et al., 2010a; 2010b).

FIELD RELATIONSHIPS

The area north of Nain has been divided into three geological units (Davoudzadeh, 1972): (I) the ophiolite-bearing coloured mélange unit cropping out with a NNW-SSE trend through the central area, (II) the Tertiary volcanic unit associated with small Tertiary dioritic intrusions in the West, and (III) the Tertiary sedimentary unit in the East (Fig. 2).

The coloured mélange in the northern part (Kuh-e-Zard area) mostly consists of Late Cretaceous limestones and Palaeocene to Early Eocene sequences (Figs. 2 and 3). Differently, in the Nain area, the coloured mélange is typically characterized by blocks of different sizes enclosed in a matrix of strongly deformed serpentinized peridotites. The blocks mainly include lithologies derived from a dismembered ophiolite sequence. The tectonic deformations that formed the mélange were responsible for disruption of the primary ophiolite sequence, and the development of multiple blocks surrounded by shear zones. However, some still preserved primary relationships among the different lithologies in the blocks can be found in the field. A reconstruction of the primary ophiolite sequence can thus be attempted, and it shows peridotites at the base covered by a crustal sequence including gabbros, sheeted dyke complex, pillow lavas and oceanic sediments. Primary relationships between pillow basalts and oceanic sediments, represented by pelagic limestones and cherts, have also been found (Fig. 4A).

The peridotites mainly consist of a thick sequence of foliated clinopyroxene-bearing harzburgites, characterized in some places by orthopyroxenite veinlets (< 10cm) (Fig. 4B) with sharp contacts with the host rocks. The mantle rocks include also minor lherzolites and dunites, showing primary relationships with the hazburgites. Impregnated peridotites are common in the field. The peridotites are generally

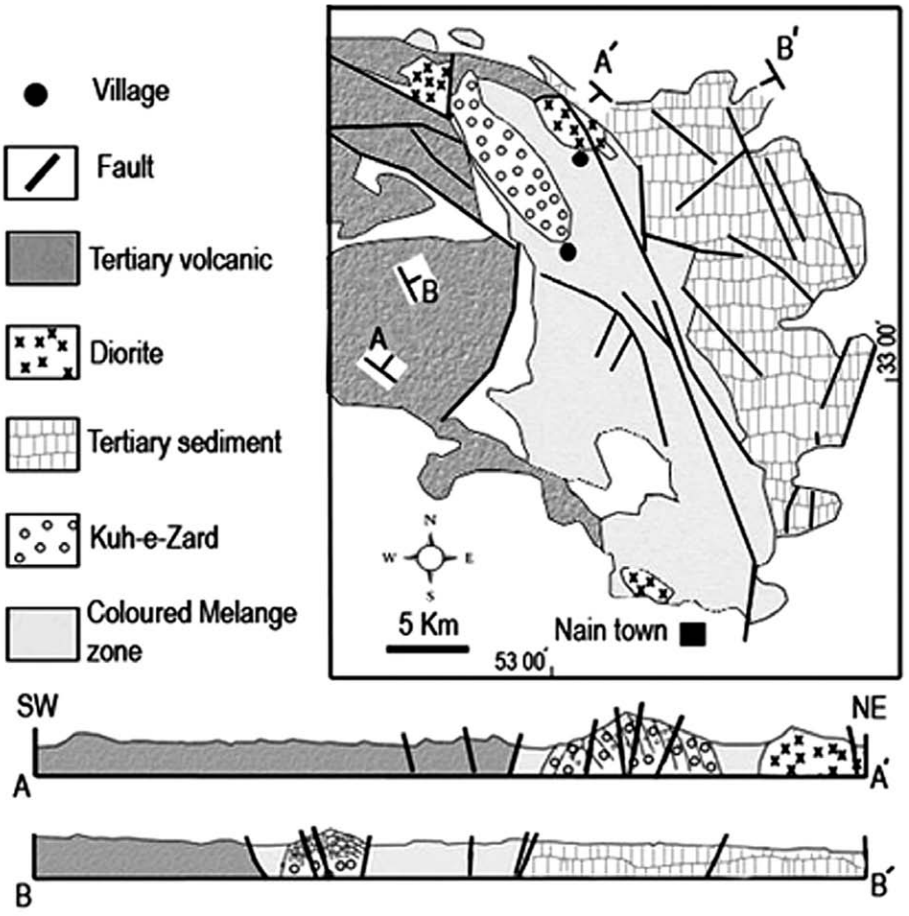

Fig. 2 - Tectonic sketch map and related cross-sections of the Nain Area (modified after Davoudzadeh, 1972).

strongly serpentinized, with increasing degree from lherzolite through harzburgite to dunite. The foliated hazburgites are cut by thin pyroxenite dykes well exposed at the southern sector of the area (Ghazi et al., 2010b). Also diabases and coarse-grain gabbroic dykes (Fig. 4E) are found in the foliated harzburgites. Their intrusive contacts with the hazburgites are sharp and regular, suggesting that the host rocks were significantly cold at the time of mafic magma intrusion. Rodingitized gabbroic dykes characterized by growth of secondary minerals such as pectolite and/or wollastonite have also been found.

The crustal rock types consist of cumulates comprising pyroxenites, websterites (Fig. 4C), wherlites, olivin-gabbronorites (Fig. 4D) and pegmatite gabbros. The pyroxenites and websterites associated with wherlites and gabbronorites occur either as dykes or as small pockets in peridotites. The crustal rocks include also pillow basalts.

In the hazburgites two types of chromitites occur in the field. The first type is chromitite patches (about 2-3 cm in size), showing sharp contacts within the harzburgites (Fig. 4G). The distances among these patches are very different, ranging in length from a few centimetres to a few meters. Their shape is mainly rounded or ovoidal. Evidence of mafic melt segregating and of minor gabbroic melt infiltrations within the peridotites around the chromitite patches has been also recognized.

The second type of chromitites occurs as large lenses (or pods) with size up to a few meters. These chromitites are surrounded by a dunite rim of ~ 1 meter thickness.

In the coloured mélange also blocks of metaophiolities and metasedimentary rocks have been found (Shirdashtzadeh et al., 2010). These rocks include marbles, skarns, schists, phyllites, quartzites, banded metacherts, amphibolites, listwaenites and metaserpentinites (Torabi et al., 2007). The mineral assemblages from metaophiolites indicate greenschist to amphibolite facies metamorphism. These metamorphic events are regarded to have occurred during the three main deformation phases developed from Jurassic to Cretaceous (Shirdashtzadeh et al., 2010). According to Rahgoshay and Shafaii Moghadam (2004) and Torabi et al. (2007), no evidence of rocks that can be interpreted as a metamorphic sole has been found.

Late Cretaceous pelagic limestones are the oldest sedimentary rocks found in the coloured mélange of the Nain area. They are massive or weakly bedded limestones, including also marls and sandstones beds, and containing both continuous and boudin-shaped radiolarian cherts. In thin sections, these rocks can be classified as Globotruncana-bearing micrites. Microfossils indicate ages ranging from Santonian-Coniacian to Campanian-Maastrichtian (Davoudzadeh, 1972). The relationships between the pelagic limestones and the other rocks of the coloured mélange are generally marked by shear zones, but in a block north of the Ahmadabad village, primary relationships between pillow lavas and red cherts interbedded with limestone layers can be observed (Fig. 4H). Therefore these deposits can be interpreted as the sedimentary cover of the ophiolites derived from the Nain oceanic basin.

The ophiolites as well as the pelagic limestones are covered by a polymict breccia with fragments of limestone, chert, volcanic rocks and serpentinite in a grey lime matrix showing a transition to a sequence of fine-grained quartzite-

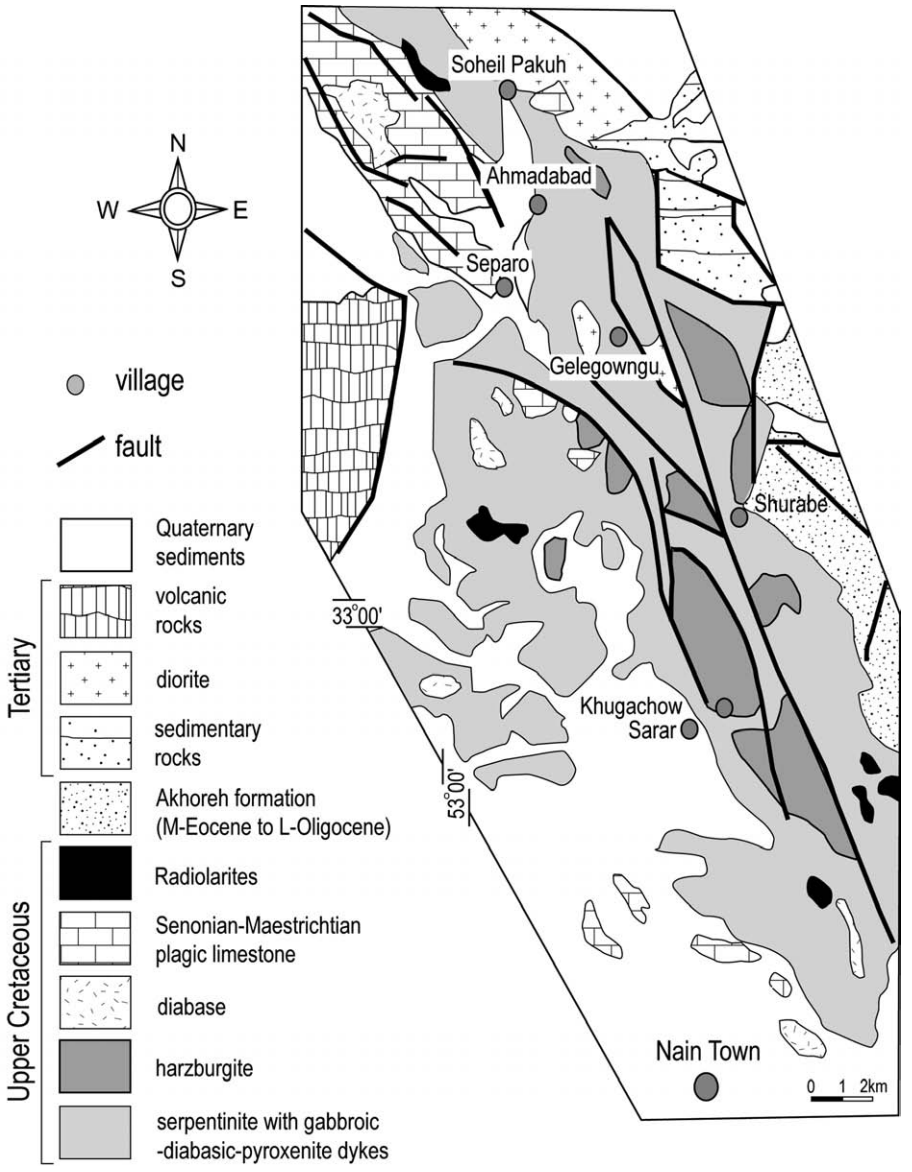

Fig. 3 - Geological map of the Nain ophiolite (modified after Davoudzadeh, 1972).

and clay-bearing neritic limestones, where interlayers of spilitic diabases have been found. The age of this succession ranges from Middle-Late Palaeocene to Early Eocene (Davoudzadeh, 1972). Thus, a sedimentation gap can be envisaged between the sedimentary cover of the ophiolites and the overlying polymict breccia. This sedimentation gap may indicate that the Paleocene to Eocene sedimentary rocks were unconformably deposited on the ophiolites after their emplacement and deformation.

PETROGRAPHY

The peridotites are mainly represented by serpentinized harzburgites, clinopyroxene-bearing harzburgites and lherzolites, whose textures dominantly consist of olivine together with large orthopyroxene porphyroclasts, small clinopyroxene porphyroclasts and tiny Cr-spinel crystals as primary minerals. Polymorphs of serpentine minerals, mainly lizardite and chrysotile, occur as secondary minerals. The peridotites show a porphyroclastic texture replaced by a mesh texture developed during serpentinization.

Harzburgites: the studied samples show various degrees of serpentinization. The main mineral is olivine (70-85 modal%), whereas orthopyroxene represents the 7-20 modal% of the rock. The minor phases are clinopyroxene (3-5 modal%) and Cr-spinel (1-3 modal%). Other minerals include sulfide minerals and Cr-chlorite (kaemmererite). A mesh texture formed due to alteration of olivine to lizardite and alteration of pyroxene to bastite. Olivine is coarse-grained and usually exhibits undulatory extinction and kink banding and it is surrounded by fine-grained olivine crystals producing a mylonitic fabric in places (Ghazi et al., 2010b). Curved olivine-olivine and olivine-pyroxene grain boundaries suggest that they were modified by partial fusion (e.g., Mercier and Nicolas, 1975). Orthopyroxenes in harzburgite can be divided into two groups. The first group is represented by porphyroclastic orthopyroxenes, displaying plastic deformation features such as undulatory extinction, kink bands, rotation, shearing, re-crystallization and lobate boundaries. The second group includes relatively smaller orthopyroxene crystals lacking the characteristics of the first group (Fig. 5A). Orthopyroxene occasionally contains very fine exsolution lamellae of clinopyroxene aligned along the mineral cleavage. Cr-spinel occurs often as subhedral to euhedral crystals (Fig. 5B).

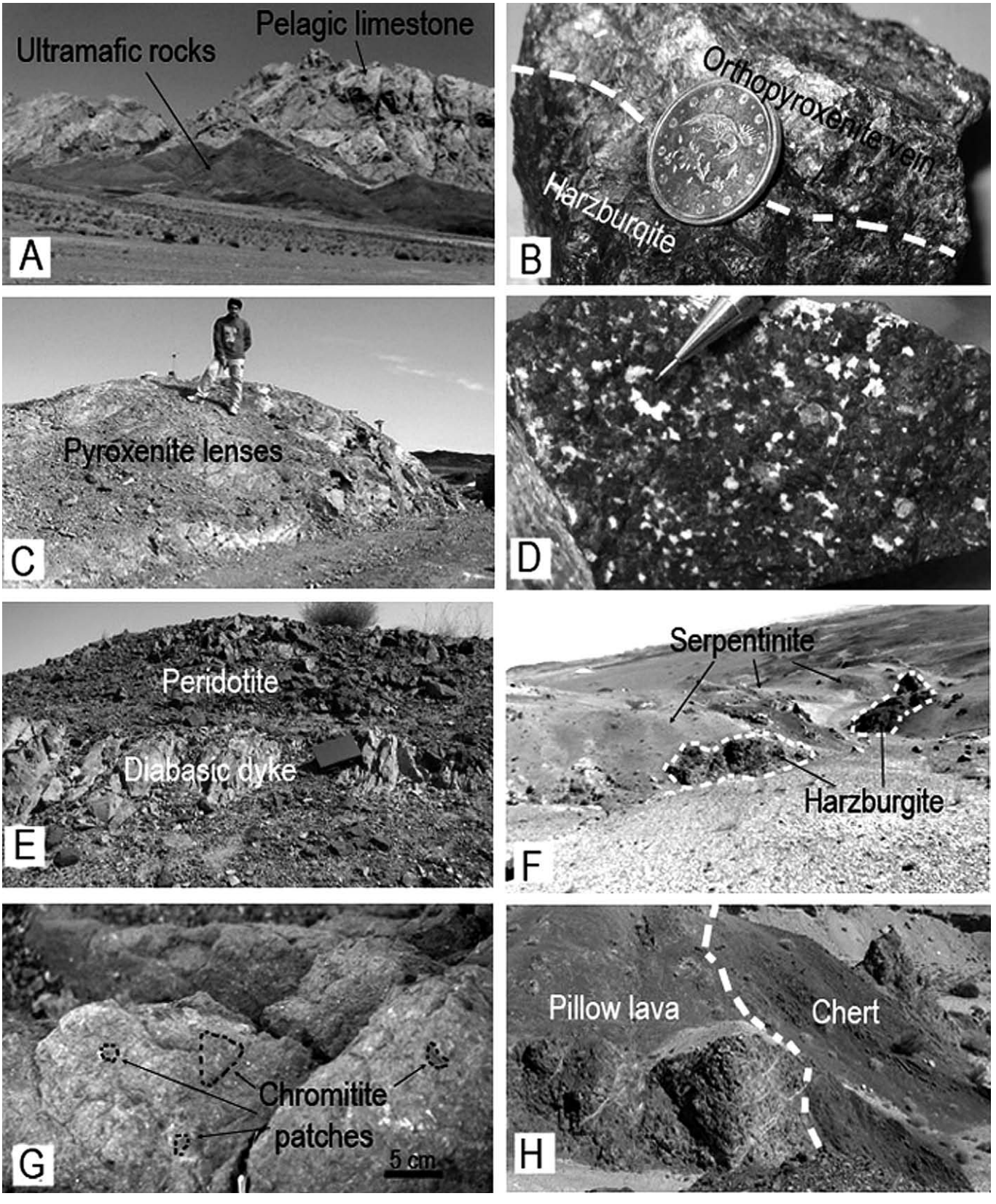

Fig. 4 - Field photos of the rock units from the Nain ophiolite, (A) Pelagic limestones overlying ultramafic rocks with normal contact, (B) Orthopyroxenite vein within harzburgites, (C) Pyroxenite lens with cumulus texture, (D) Olivine gabbronorites with dendritic aggregation of white plagioclase, (E) Diabasic dyke within peridotites, (F) Serpentinized peridotites, (G) Chromitite patches in peridotites, (H) Normal contact between Upper Cretaceous cherts and pillow lavas.

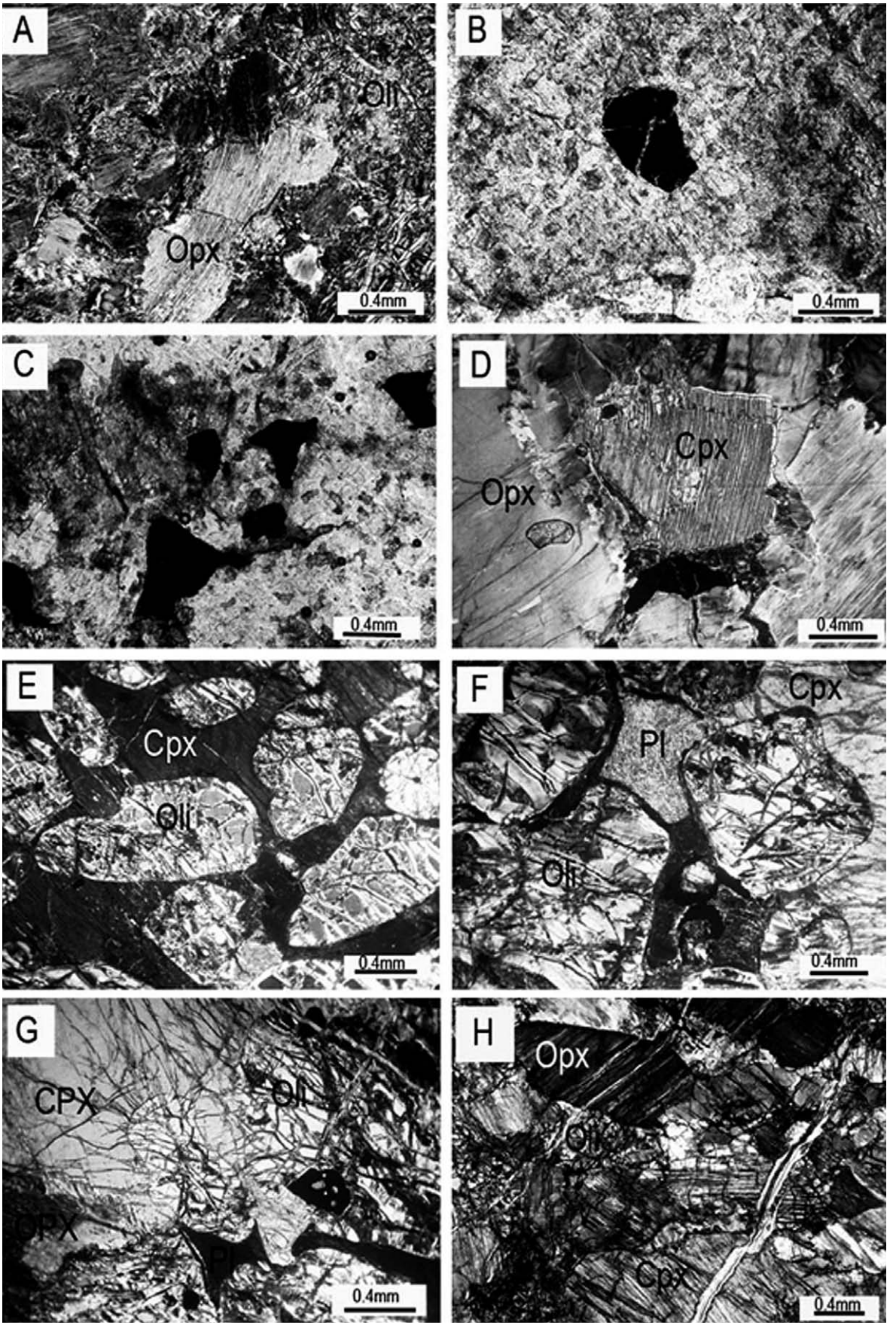

Fig. 5 - Photomicrographs of the Nain mantle rocks. (A) Kink bands in orthopyroxene (Opx) from harzburgites, (B,C) chromite (Cr-spinel) crystals and serpentinized olivine (Oli) and orthopyroxene (Opx), (D) Clinopyroxenes (Cpx) within orthopyroxenite, (E) poikilitic olivine grains in large clinopyroxene porphyroclast in wehrlites, (F) curved contacts between olivine-olivine, secondary plagioclase (Pl) and clinopyroxene in the olivine gabbros, (G) olivine, orthopyroxene, secondary plagioclase (Pl) and clinopyroxene in olivine gabbronorites, (H) olivine, orthopyroxene and clinopyroxene in websterites.

Lherzolites: the studied samples contain ≈ 70 modal% olivine, ≈ 20 modal% orthopyroxene, < 10 modal% clinopyroxene and 2-3 modal% Cr-spinel. The lherzolites show both mosaic and porphyroclastic textures. Clinopyroxene appears as banded exsolution lamellae and small inclusions in orthopyroxene and as small crystals among olivines and orthopyroxene (Ghazi et al., 2010b). Some orthopyroxene and clinopyroxene crystals show kink structure.

Dunites: this lithotype hosts chromitite with high Cr content (chromitite samples HA1 and HA2). Subhedral to euhedral crystals of Cr-spinel show thick ferroan Cr-spinel rims (Fig. 5C). Olivine forms porphyroclastic grains with 120° triple junctions. Scarce chlorite and talc represent products of alteration of orthopyroxene.

Chromitites: as previously described, the chromitites in the Nain ophiolites occur as both chromitite patches hosted in harzburgite and chromitite lenses rimmed by dunite.

The chromitite patches include 10-15 modal% Cr-spinel and less than 3 modal% pyroxene. Olivine and serpentinite minerals also occur as minor phases. Cr-spinel appears as crystals from 0.5 to 4 mm long within a silicate (mainly olivine or serpentine) phase. Cr-spinel crystals are aligned parallel to the rock foliation. Some Cr-spinel grains show rounded boundaries.

The chromitite lenses contain 10-40 modal% Cr-spinel, with an increase of this percentage in the inner parts of the lenses. The size of Cr-spinels is larger in the lenses. These rocks lack pyroxene.

Orthopyroxenite veins: the studied samples typically show < 5% olivine and minor amounts of clinopyroxene (< 2%), Cr-spinel and traces of amphibole (Fig. 5D). These veins have variably deformed cumulus textures in the core and generally oriented minerals (more likely due to magmatic flow) at the contact with the harzburgitic host.

Cumulates: in some ultramafic cumulates, olivine crystals exhibit rounded edges and clinopyroxene (25-50 modal%) appears as the inter-cumulus phase (Fig. 5E). Based on the clinopyroxene percentage, the rocks can be divided into wherlites and olivine-clinopyroxenites. Some other mafic cumulate rocks contain plagioclase and rare orthopyroxene along with clinopyroxene and olivine. These can be classified as olivine gabbronorite and olivine gabbro (Fig. 5F and G). In these rocks, also rounded olivine crystals make the cumulus phase and clinopyroxene, plagioclase and rare orthopyroxene are inter-cumulus phases. Textural relationships indicate that plagioclase crystallized after clinopyroxene, a feature indicative of suprasubduction zone magmatic sequences.

Clinopyroxenites and websterites are the other types of cumulate rocks. Cumulus phase is clinopyroxene and inter-cumulus phases are clinopyroxene, orthopyroxene and rare (> 5 modal%) olivine (Fig. 5H). The inter-cumulus phases are less than 7% and the cumulus phases are in mutual contact. Cr-spinel and iron oxides make about 2% of the rocks.

CHEMICAL ANALYSES

The ICP-MS and ICP-AES analyses were performed on well-defined representative samples at the Centre de Géochimie de la surface, Strasbourg, France. The analytical precision for major elements is better than 5% and for trace elements was found to be better than 5%, for larger than 5 ppm concentration in the samples. Major elements and Ni, Cr, V, Sc, Y, Zr, Ba, Sr were measured by ICP-AES, whereas other trace and rare earth elements were determined by ICP-MS. Electron microprobe analyses of the polished samples were carried out using a Cameca SX-50 superprobe, at Université Nancy I, France. The accelerating voltage and beam current were 12keV and 10nA respectively. Natural and synthetic standards were used for calibration.

WHOLE ROCK CHEMISTRY

Seven representative samples from the peridotites (harzburgite and lherzolite) were chosen for analysis. Table 1 includes the whole rock chemistry of the representative peridotite samples from the Nain area. The SiO_2 contents of the peridotites range between 36.50 to 40.70wt%. All Fe is assumed to be FeO. The analyzed samples are rich in MgO (30.0-43.30wt%), with a wide range in concentration of Al_2O_3 (0.8-7.20wt%), CaO (0.50-7.10wt%) and TiO_2 (0.01-0.04wt%). Al_2O_3 is expected to be the most immobile major element in serpentinized peridotites (Snow and Dick, 1995); also Al_2O_3 abundance increases from harzburgite to lherzolite samples. CaO abundance is generally correlated with increasing clinopyroxene abundance (Casey, 1997), because clinopyroxene is the main CaO-bearing phase in these rocks. Therefore the high amounts of CaO and Al_2O_3 in the Nain peridotites show high amount of modal clinopyroxene in the original samples and a low degree of serpentinization. Clear positive correlations between CaO-Al_2O_3, CaO-Sc and CaO-Y most likely indicate that the abundance of these elements is controlled by the amount of clinopyroxene in the rocks. On the other hand, low amounts of CaO and high amounts of LOI in some studied peridotites may be attributed to the high degree of serpentinization. Relatively high loss on ignition (LOI) confirms extensive serpentinization of these rocks. Based on petrography and geochemistry, two samples (BKSh-12 and BY23) most likely represent cumulitic peridotites rather than mantle peridotites. In fact, the amount of CaO in these samples, as well as the Al content in sample By23 are too high for mantle peridotites. On the basis of the modal composition, all the investigated samples fall within the harzburgite and lherzolite fields (Fig. 6).

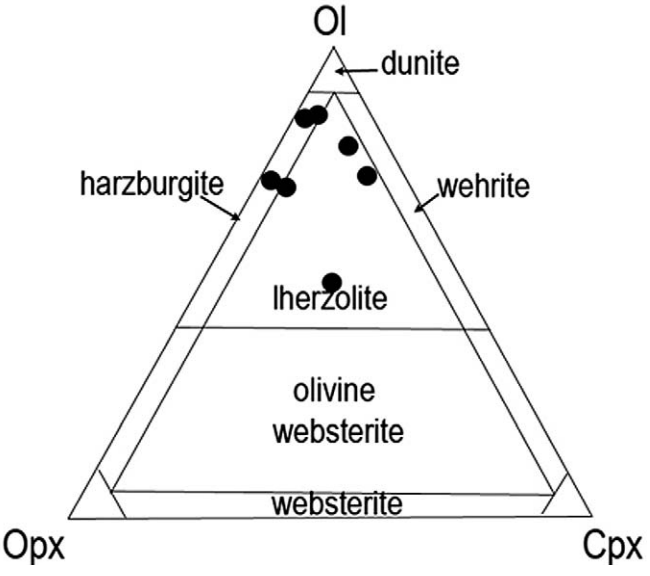

Fig. 6 - Normative mineral composition of the Nain peridotites plotted on the olivine (Ol), orthopyroxene (Opx) and clinopyroxene (Cpx) triangular diagram.

Table 1 - Whole rock chemistry of the representative samples from the Nain peridotites. BDL (belw derection limits).

Sample	BKB-1	BKB-7	BPV-12	BSU-14	BKSh-12	BKB-12	BY23
SiO_2	36.50	40.70	39.10	38.00	40.49	38.67	38.90
TiO_2	0.01	0.02	0.03	0.02	0.04	0.03	0.04
Al_2O_3	1.14	0.81	1.99	1.12	2.93	2.02	7.27
FeOt	7.63	8.22	7.86	8.04	8.93	8.14	7.82
CaO	1.15	0.76	2.03	0.59	6.33	3.17	7.13
Na_2O	0.03	0.05	BDL	0.20	0.01	0.01	0.23
MgO	41.70	43.30	39.30	42.90	31.80	37.63	30.50
K_2O	0.13	0.07	0.13	0.18	0.00	0.88	0.00
MnO	0.10	0.12	0.11	0.11	0.13	0.11	0.12
P_2O_5	0.01	0.05	0.03	0.05	0.01	0.02	0.05
LOI	10.79	5.35	8.95	8.00	8.80	9.50	7.57
Total	99.21	99.31	99.52	99.12	99.12	99.12	99.69
Ba	4	5	7	2	6.360	5.787	7.330
Rb	0.216	0.228	0.21	0.174	0.23	0.218	0.594
Sr	17	19	13	4	19.2	16.4	170
Y	0.922	2	0.928	2	2.209	1.353	2.77
Zr	1.74	9	0.561	9	1.337	1.212	3.98
Nb	0.051	0.01	0.03	0.372	0.023	0.034	0.015
Th	0.05	0.023	0.022	0.022	0.017	0.029	BDL
Pb	1.52	0.892	1.63	1.72	1.68	1.61	0.608
Zn	57	48	57	39	47.9	53.9	65.7
Cu	3.76	29.5	19.1	12.5	23.783	15.547	113
Ni	1851	2097	1809	1946	993.377	1551.21	1268
V	41	55	65	46	76.513	60.837	56
Cr	1732	2828	2294	2421	2915.28	2313.76	4119
Hf	0.028	0.023	0.018	0.027	0.033	0.0263	0.056
Cs	0.01	0.023	BDL	0.012	BDL	0.018	BDL
Sc	9	11	12	10	21.65	14.216	15.2
Ta	0.013	BDL	0.002	BDL	0.001	0.005	0.36
Co	111	124	107	96.4	84.80	100.93	106
U	0.029	0.051	0.042	0.076	0.020	0.030	0.033
W	0.617	0.303	0.224	0.230	0.013	0.284	2.62
La	0.051	BDL	BDL	BDL	1.461	BDL	BDL
Ce	0.125	0.05	BDL	0.02	0.108	0.08	0.061
Pr	0.012	0.012	0.001	0.006	0.016	0.009	0.016
Nd	0.082	0.04	0.023	0.02	0.097	0.067	0.143
Sm	0.031	0.03	0.015	0.021	0.058	0.034	0.099
Eu	0.008	0.009	0.014	0.005	0.036	0.019	0.054
Gd	0.032	0.051	0.052	0.013	0.113	0.065	0.21
Tb	0.007	0.006	0.016	0.006	0.017	0.013	BDL
Dy	0.08	0.074	0.126	0.052	0.188	0.131	0.29
Ho	0.021	0.024	0.035	0.015	0.042	0.032	0.067
Er	0.068	0.069	0.124	0.043	0.111	0.101	0.18
Tm	0.008	0.01	0.027	0.007	0.022	0.019	0.031
Yb	0.084	0.093	0.17	0.065	0.12	0.124	0.186
Lu	0.015	0.018	0.028	0.012	0.019	0.02	0.025

Variations of selected oxides in the Nain peridotites are shown in Fig. 7. SiO_2, Al_2O_3, FeO, and CaO are plotted against MgO. The composition of primitive mantle (McDonough and Sun, 1995) is included for comparison. SiO_2 content of the Nain ophiolites is relatively lower than in primitive mantle. The positive correlation of FeO with MgO may reflect the influence of cumulate processes involving relatively Fe-rich olivine (e.g., Medaris et al., 2005; Fig. 7). Samples BKSh-12 and BY23 show a positive correlation between FeO and MgO (i.e., cumulitic nature) and they are completely different from other samples where that correlation is negative (i.e., mantle peridotites).

The primitive mantle normalized incompatible trace element patterns for the peridotites are shown in Fig 8. All peridotites show high amounts of Pb and U. Additionally, they do not show a refractory nature, confirmed by rather high contents of Ba, Rb, Th, Zr, Sr, U, Pb and Y (Fig. 8A). The chondrite-normalized REE patterns for the Nain peridotites are shown in Fig. 8B. All samples exhibit depletion in all rare earth elements (REE). Depletion in light rare earth elements (LREE) is more pronounced compared to that of heavy rare earth elements (HREE).

CR-SPINELS CHEMISTRY

The cores of fresh Cr-spinel grains were analyzed. The Fe^{3+} and Fe^{2+} contents of the minerals were calculated based on stoichiometric criteria. Table 2 provides representative analyses of Cr-spinels. The microprobe data from dunites used in the mineral chemistry of Cr-spinels are from Torabi and Pirnia (2008). Compositions of Nain Cr-spinels are compared with other Cr-spinels from known tectonic settings (Table 3; Stowe, 1994).

Chemistry of Cr-spinels in chromitite patches and host harzburgite

Samples 1, 2 and 3 represent the Cr-spinels analysed from chromitite patches. The TiO_2, Al_2O_3 and MgO contents of these Cr-spinels range between 0.22-0.40, 18.90-22.20 and 12.50-15.00wt% respectively. Also the Cr/Fe_{total} ratio for this type of Cr-spinels is 2.60 to 3.30. These Cr-spinels plot in the ophiolite-related spinels field in the Cr-Al-Fe^{3+} diagram (Fig. 9A) and they also plot in the field of podiform chromite originated from the mantle, in the Al_2O_3 versus Cr_2O_3 diagram (Fig. 9B). The CaO, FeO and MnO contents are < 0.1, 13.80-17.20 and < 0.3wt%, respectively. The Cr# versus the Mg# of the Cr-spinels from the chromitite patches plot in the podiform chromite field in the diagram of Fig. 9C.

Cr-spinels from the host harzburgite have Mg# of 60.93-67.42, Al_2O_3 content of 32-34.17wt% and TiO_2 content of 0.00-0.12wt%. Cr# is low in this type of Cr-spinel (39.64-41.55). The CaO, FeO and MnO contents are about 0.03>, 17 and 0.3wt%, respectively. These Cr-spinels are of residual peridotite/ophiolite spinel types (Fig. 9A), which are originated in the mantle (Fig. 9B) and plot in the abyssal and back-arc peridotite fields in Fig. 9C.

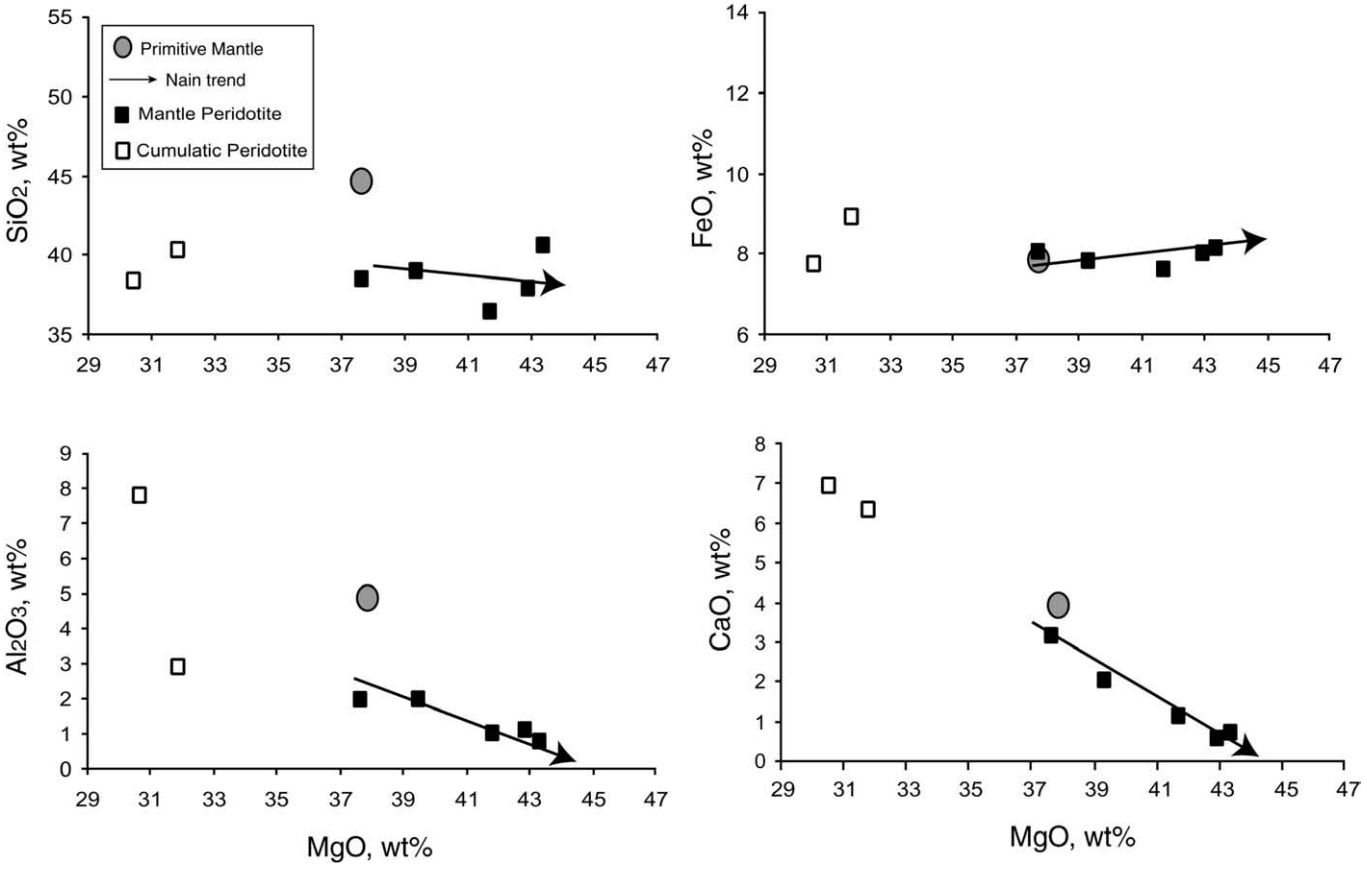

Fig. 7 - Variation diagrams of Al_2O_3, CaO, SiO_2 and FeO versus MgO in peridotites of the Nain ophiolite. For more explanation see text.

Table 2 - Microprobe analyses of Cr-spinels from chromitite, harzburgite and dunite in the Nain ophiolite. Data from Torabi and Pirnia (2008) are indicated by an asterisk.

Rock type	Chromitite patches																
Sample	Chromitite (1)					Chromitite (2)					Chromitite (3)						
SiO_2	0.00	0.01	0.03	0.75	0.00	0.00	0.05	0.04	0.00	0.70	0.01	0.00	0.00	0.00	0.00	0.00	0.10
TiO_2	0.22	0.33	0.30	0.24	0.13	0.33	0.24	0.28	0.29	0.26	0.23	0.32	0.20	0.40	0.36	0.25	0.28
Al_2O_3	20.76	20.48	20.52	18.90	20.13	21.21	22.20	22.37	20.46	21.52	20.33	20.87	18.91	20.41	20.71	20.80	20.23
$FeO^{(T)}$	13.82	14.09	15.06	15.71	15.21	15.97	14.95	14.69	14.65	14.62	15.16	14.66	17.28	15.65	15.42	15.79	15.59
MnO	0.01	0.10	0.13	0.16	0.23	0.11	0.19	0.23	0.05	0.19	0.15	0.29	0.23	0.17	0.18	0.21	0.07
MgO	13.76	13.97	13.78	14.00	14.79	13.99	14.70	13.69	14.10	15.09	14.17	13.85	12.82	13.60	13.59	12.85	12.89
CaO	0.04	0.00	0.03	0.18	0.07	0.00	0.01	0.00	0.00	0.17	0.02	0.00	0.00	0.00	0.03	0.00	0.00
Na_2O	0.02	0.02	0.00	0.03	0.01	0.01	0.05	0.00	0.03	0.01	0.03	0.00	0.00	0.06	0.01	0.02	0.00
K2O	0.01	0.01	0.00	0.00	0.02	0.00	0.00	0.01	0.00	0.00	0.01	0.03	0.00	0.00	0.00	0.00	0.04
Cr_2O_3	49.76	49.68	48.77	49.07	48.86	48.09	48.18	47.83	48.78	46.67	49.09	48.94	48.84	47.83	48.82	48.74	49.48
NiO	0.00	0.00	0.00	0.00	0.00	0.00	0.00	0.00	0.00	0.00	0.00	0.00	0.00	0.00	0.00	0.00	0.00
Total	98.40	98.69	98.62	99.05	99.45	99.71	100.57	99.14	98.36	99.23	99.20	98.96	98.28	98.12	99.12	98.66	98.68
Atoms to 4 oxygens																	
Si	0.000	0.000	0.001	0.023	0.000	0.000	0.001	0.000	0.000	0.021	0.000	0.000	0.000	0.000	0.000	0.000	0.003
Ti	0.005	0.008	0.007	0.006	0.003	0.008	0.005	0.006	0.007	0.006	0.005	0.008	0.005	0.009	0.009	0.006	0.007
Al	0.764	0.751	0.754	0.694	0.730	0.768	0.792	0.813	0.752	0.768	0.742	0.763	0.705	0.754	0.758	0.768	0.748
Fe^{3+}	0.000	0.010	0.029	0.040	0.075	0.047	0.041	0.008	0.032	0.061	0.045	0.021	0.064	0.041	0.027	0.014	0.005
Fe^{2+}	0.363	0.357	0.363	0.369	0.316	0.363	0.338	0.371	0.350	0.309	0.346	0.359	0.394	0.369	0.374	0.400	0.405
Mn	0.000	0.003	0.003	0.004	0.006	0.003	0.005	0.006	0.001	0.005	0.004	0.008	0.006	0.004	0.005	0.006	0.002
Mg	0.640	0.648	0.640	0.650	0.678	0.641	0.663	0.630	0.655	0.681	0.654	0.641	0.605	0.635	0.628	0.600	0.603
Ca	0.001	0.000	0.001	0.006	0.002	0.000	0.001	0.000	0.000	0.032	0.001	0.000	0.000	0.000	0.001	0.000	0.000
Na	0.001	0.001	0.000	0.002	0.001	0.001	0.003	0.000	0.002	0.001	0.002	0.000	0.000	0.004	0.001	0.001	0.000
K	0.000	0.000	0.000	0.000	0.001	0.000	0.000	0.000	0.00	0.000	0.002	0.001	0.000	0.000	0.000	0.000	0.002
Cr	1.228	1.223	1.201	1.208	1.188	1.169	1.153	1.166	1.202	1.117	1.201	1.201	1.222	1.185	1.199	1.207	1.227
Ni	0.000	0.000	0.000	0.000	0.000	0.000	0.000	0.000	0.000	0.000	0.000	0.000	0.000	0.000	0.000	0.000	0.000
Total	3.002	3.001	2.999	3.002	3.000	3.000	3.002	3.000	3.001	3.001	3.002	3.002	3.001	3.001	3.002	3.002	3.002
Cr#	61.650	61.938	61.452	63.530	61.954	60.339	59.280	58.915	61.529	59.264	61.830	61.139	63.404	61.125	61.264	61.118	62.134
Fe^{3+}#	0.000	0.005	0.015	0.020	0.038	0.024	0.020	0.004	0.016	0.031	0.023	0.011	0.032	0.021	0.013	0.007	0.002
Fe^{3+}/Fe^{2+}	0.000	0.027	0.080	0.109	0.237	0.130	0.120	0.022	0.091	0.197	0.132	0.059	0.161	0.111	0.071	0.034	0.011
Mg#	63.780	64.488	63.804	63.800	68.198	63.831	66.260	62.925	65.183	68.769	65.350	64.092	60.571	63.245	62.722	59.995	59.851
Cr/Fe^{tot}	3.379	3.333	3.061	2.953	3.036	2.847	3.047	3.076	3.147	3.018	3.061	3.156	2.671	2.888	2.992	2.917	3.001
$Fe^{2+}/(Fe^{2+}+Fe^{3+})$	1.000	0.973	0.925	0.901	0.808	0.885	0.893	0.979	0.916	0.836	0.884	0.944	0.861	0.900	0.933	0.967	0.989

Table 2 - (*continued*)

Rock type	Chromitite lenses								Harzburgite								Dunite*	
sample	Chromitite (HA1)					Chromitite (HA2)			1	2	3	4	5	6	7	8	1	2
SiO_2	0.13	0.12	0.08	0.11	0.11	0.14	0.14	0.17	0.06	0.03	0.03	0	0	0.03	0	0	0	0
TiO_2	0.25	0.19	0.2	0.22	0.18	0.28	0.27	0.28	0.04	0.04	0.09	0.12	0.01	0.02	0	0.06	0.43	0.49
Al_2O_3	13.85	13.6	13.75	13.8	14	15	14.13	14.7	32	32.72	33.01	34.17	33.28	32.76	32.54	32.31	26.8	27.03
FeO(T)	14.6	14.9	14.83	14.8	14.76	15.01	15	14.8	18.93	17.17	17.8	16.81	17.2	16	16.2	16.67	23.79	23.13
MnO	0.2	0.24	0.27	0.27	0.22	0.2	0.21	0.25	0.23	0.25	0.18	0.2	0.24	0.26	0.02	0.27	0.29	0.3
MgO	15	14.95	14.97	15.05	14.83	15.4	15.01	14.8	13.73	13.88	13.83	14.63	14.24	15.24	15.09	15.03	11.87	12.17
CaO	0.02	0.01	0	0	0.01	0.02	0.02	0.03	0	0	0	0.03	0.02	0	0	0	0.01	0
Na_2O	0.01	0.02	0.01	0	0.02	0.03	0.03	0.04	0.05	0.01	0	0.04	0	0.1	0.03	0.03	0	0
K_2O	0.01	0	0.01	0	0	0.02	0.02	0.03	0.02	0	0	0.03	0	0	0.01	0	0	0
Cr_2O_3	54.85	54.77	55.03	54.48	54.65	53.9	53.3	52.9	33.91	34.05	33.06	33.45	33.13	33.71	34.37	33.88	35.96	36.26
NiO	0	0	0	0	0	0.1	0.11	0.16	0.16	0.14	0.18	0.18	0.24	0.18	0.32	0.24	0	0
Total	98.92	98.8	99.15	98.73	98.78	100.1	98.24	98.16	99.11	98.28	98.17	99.66	98.35	98.3	98.57	98.48	99.14	99.38
Atoms to 4 oxygens																		
Si	0.005	0.005	0.003	0.004	0.004	0.005	0.005	0.006	0.002	0.001	0.001	0	0	0.001	0	0	0	0.001
Ti	0.007	0.005	0.006	0.006	0.005	0.007	0.007	0.007	0.001	0.001	0.002	0.003	0	0.001	0	0.001	0.01	0.011
Al	0.49	0.485	0.51	0.51	0.54	0.574	0.508	0.52	1.118	1.147	1.157	1.172	1.16	1.138	1.13	1.124	0.965	0.966
Fe^{3+}	0.08	0.091	0.086	0.091	0.09	0.091	0.09	0.091	0.08	0.047	0.058	0.05	0.061	0.071	0.064	0.08	0.146	0.136
Fe^{2+}	0.3	0.32	0.311	0.31	0.321	0.315	0.318	0.311	0.389	0.38	0.384	0.359	0.364	0.323	0.335	0.332	0.461	0.452
Mn	0.005	0.006	0.007	0.007	0.005	0.005	0.005	0.006	0.006	0.006	0.004	0.006	0.006	0.006	0	0.007	0.001	0.001
Mg	0.71	0.7	0.696	0.72	0.71	0.73	0.72	0.7	0.606	0.615	0.613	0.635	0.628	0.669	0.663	0.661	0.54	0.551
Ca	0.001	0	0	0	0	0.001	0.001	0.001	0	0	0	0.001	0.001	0	0	0	0	0.001
Na	0.001	0.001	0.001	0	0.001	0.002	0.002	0.002	0.003	0	0	0.002	0	0.006	0.001	0.001	0	0
K	0	0	0	0	0	0.001	0.001	0.001	0.001	0	0	0.001	0	0	0	0	0	0
Cr	1.316	1.314	1.32	1.3	1.311	1.293	1.279	1.269	0.794	0.8	0.777	0.77	0.775	0.785	0.801	0.79	0.869	0.872
Ni	0	0	0	0	0	0.002	0.003	0.003	0.004	0.003	0.004	0.004	0.006	0.004	0.008	0.006	0	0
Total	2.915	2.927	2.94	2.948	2.987	3.026	2.939	2.917	3.004	3	3	3.003	3.001	3.004	3.002	3.002	2.992	2.991
Cr#	72.8	73	72.1	71.8	70	69.2	71.5	70	41.551	41.109	40.187	39.64	40.044	40.833	41.47	41.295	47.372	61.05
Fe^{3+}#	0.042	0.048	0.044	0.047	0.046	0.046	0.047	0.048	0.0402	0.024	0.029	0.025	0.031	0.035	0.032	0.04	0.074	0.087
Fe^{3+}/Fe^{2+}	0.26	0.28	0.27	0.3	0.28	0.29	0.28	0.29	0.206	0.125	0.151	0.138	0.168	0.219	0.193	0.24	0.316	0.3
Mg#	70.2	68.6	69.1	70	68.8	69.8	68.3	68.2	60.929	61.838	61.46	63.864	63.283	67.419	66.452	66.593	53.935	54.943
Cr/Fe_{tot}	3.46	3.19	3.32	3.24	3.18	3.18	3.13	3.15	1.694	1.874	1.755	1.881	1.821	1.991	2.006	1.921	1.429	1.482
$Fe^{2+}/Fe^{2+}+Fe^{3+}$	0.79	0.778	0.783	0.773	0.781	0.775	0.78	0.773	0.829	0.889	0.868	0.878	0.856	0.82	0.838	0.806	0.76	0.769

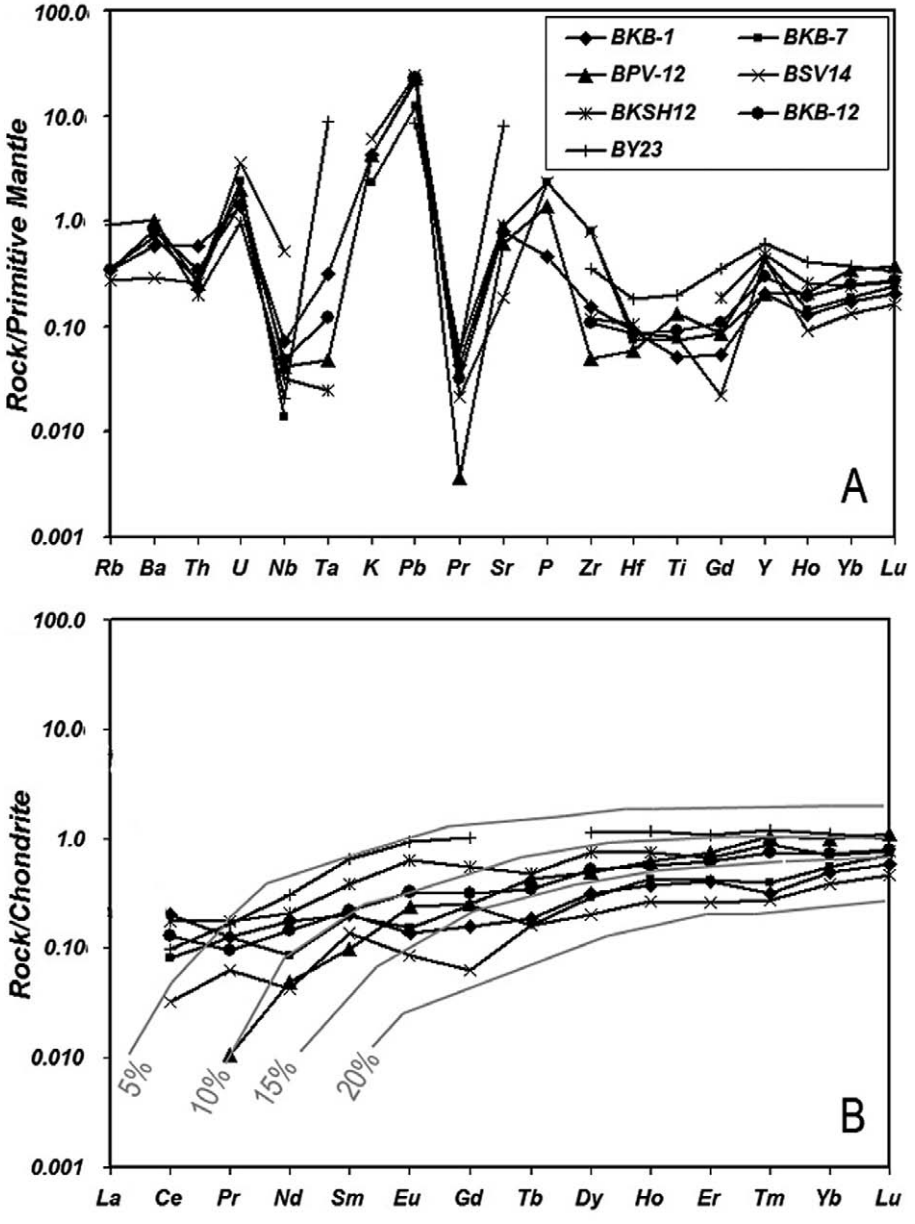

Fig. 8 - (A) Pattern for incompatible elements from the Nain peridotites normalized to primitive mantle. (B) Chondrite-normalized REE patterns for the Nain peridotites. Normalizing values are from Sun and McDonough (1989). Calculated fractional melting curves (light grey) are from Niu (1997).

Chemistry of Cr-spinels in chromitite lenses and host dunite

Samples HA1 and HA2 represent the Cr-spinels analyses from the chromitite lenses. TiO_2, Al_2O_3, and MgO contents of these Cr-spinels are between 0.18-0.28, 13.60-14.70 and 14.80-15.05wt%, respectively. Cr/Fe_{total} is 3.13-3.46 and they plot in the ophiolite related spinels field in Fig. 9A, and in the podiform chromites field in Fig. 9B and C. The CaO, FeO and MnO contents are < 0.03, 14.6-15.01 and < 0.27wt%, respectively. The Cr# versus Mg# of Cr-spinels from the chromitite lenses plot in the podiform chromitite field in the diagram of Fig. 9C. Dunite around the chromitite lenses contains Cr-spinel crystals with Mg# ~ 54. Al_2O_3 content of this Cr-spinel is ~ 27wt% and TiO_2 content is relatively high (~ 0.4wt%). The Cr# is relatively low (~ 47-61). FeO content is ~ 23wt% and MnO content is ~ 0.30wt%. These Cr-spinels plot in the residual peridotite/ophiolite field in Fig. 9A. Cr-spinel in dunite also shows a mantle origin (Fig. 9B). These Cr-spinels cluster at the low- Mg# end of the diagram of Cr# versus Mg# (Fig. 9C).

DISCUSSIONS

Nature of the parental melts

Whole rock Tb/Yb versus Al_2O_3 contents for the studied peridotites indicate that partial melting of the source materials occurred within the spinel melting field in the mantle (Fig. 10).

The chemical composition of Cr-spinel is used to constrain the chemistry of the parental melt (e.g., Auge, 1987). We calculated the Al_2O_3 content of the parental melt using the equation of Maurel and Maurel (1982), which is:

$$(Al_2O_3)_{spinel} = 0{\cdot}035(Al_2O_3)^{2.42}_{melt}\ (Al_2O_3 \text{ in wt\%})$$

The Al_2O_3 content of the parental melt is 13.58-13.87wt% for the chromitite patches and 11.58-11.95 for the lenses (Table 4). This indicates a boninitic nature for the chromitite crystallizing magma. Al_2O_3 contents calculated using the chemistry of Cr-spinels in dunite and harzburgite are 15.5wt% and 16.7wt%, respectively. The FeO/MgO ratio in

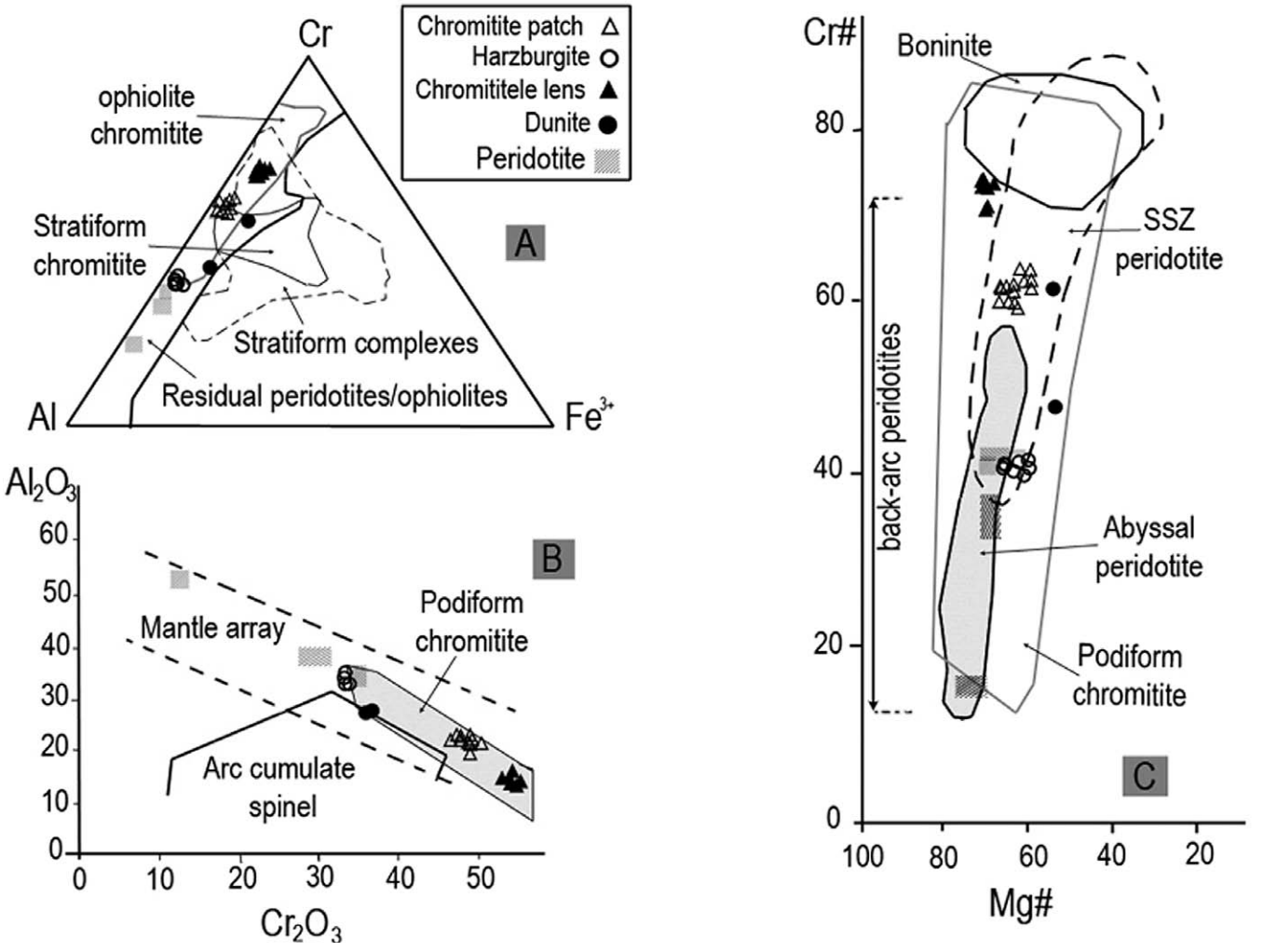

Fig. 9 - (A) Ternary plot of Cr-Al-Fe^{3+} in Cr-spinels from chromitite, dunite and harzburgite. The superimposed fields are taken from Jan and Windley (1990) and the fields of chromitites are from Proenza et al. (2007); (B) Al_2O_3 versus Cr_2O_3 diagram for the chromitites to determine their origin and type. Spinel fields are from Conrad and Kay (1984), Haggerty (1988) and Kepezhinskas et al. (1995), and chromite types are after Bonavia et al. (1993); (C) Cr# versus Mg# diagram for the studied spinels. The podiform and stratiform fields are from Irvine (1967) and Leblanc and Nicolas (1992), the boninitic field from Arai (1992), the abyssal peridotite field from Dick and Bullen (1984), back-arc peridotite field from Monnier et al. (1995) and SSZ peridotite field from Choi et al. (2008). Peridotite data shown with filled symbols in this figure and other graphs are from Ghazi (2010b).

Table 3 - Comparison of Cr-spinel compositions from the Nain complex with Cr-spinels from other known tectonic settings (data from Stowe, 1994).

Deposits	$Mg/Mg+Fe^{2+}$	Cr/Cr+Al	Cr/Fe_{tot}	Fe^{3+}/Fe^{2+}	Ti^{4+} (4 oxygen basis)
Nain chromitite patches	0.58-0.63	0.59-0.68	2.6-3.3	0.00-0.23	0.003-0.008
Nain chromitite lenses	0.68-0.70	0.69-0.73	3.13-3.46	0.26-0.30	0.005-0.007
Archaen ultramafic-mafic complex of Selukwe	0.68-0.78	0.72-0.77	2.7-4.8	0.00-0.25	0.06-0.10
Contintal Layered Complex:					
Bushveld	0.24-0.58	0.60-0.75	0.95-3.0	0.16-1.12	0.13-1.06
Great Dyke	0.36-0.67	0.70-0.80	2.1-3.9	0.14-0.26	0.02-0.13
Ophiolite segregated (Layered Cumulates):					
Cyprus (stratiform)	0.47-0.74	0.52-0.84	1.9-3.8	0.02-0.48	0.02-0.04
Ophiolite podiform (Tectonic mantle):					
Semail (Oman)	0.47-0.71	0.11-0.80	0.8-3.9	0.00-0.24	0.01-0.04

the parental melt has also been estimated from the FeO/MgO ratio of Cr-spinel using the empirical formulation of Auge (1987), which is:

$$\ln(FeO/MgO)_{Spinel} = \\ = 0{\cdot}47 - 1{\cdot}07XAl_{Spinel} + 0{\cdot}64XFe^{3+}{}_{Spinel} + \ln(FeO/MgO)_{melt}$$

where

$$XAl_{Spinel} = \\ = Al/(Al + Cr + Fe^{3+}) \text{ and } XFe^{3+}{}_{Spinel} = \\ Fe^{3+}/(Al + Cr + Fe^{3+}).$$

The FeO/MgO values are estimated to be 0.99-1.1 for the chromitite patches and 0.8 for the chromitite lenses. It is 1.6 for dunite and 1.3 for harzburgite (Table 4). The host rocks (dunite and harzburgite) do not indicate an unequivocal nature for the parental melts using the calculations mentioned above, but the chemistry of chromitites (both patches and lenses) shows a bonintic composition for the parental melt. The plot of Cr# versus TiO_2 wt% (Fig. 11) shows that the Cr-spinels in chromitite lenses plot in the boninitic field and the Cr-spinels in harzburgite plot in the highly depleted and depleted peridotite fields, whereas the Cr-spinels in dunite and chomitite patches plot among the boninite, MORB and depleted peridotite fields.

Re-equilibration of Fe and Mg between silicates and spinel may change these values considerably. The partitioning of Mg and Fe between coexisting Cr-spinel and olivine has been widely used as a geothermometer (Irvine, 1965). The estimated temperature for the studied dunite is ~ 900ºC, on the basis of the olivine-spinel thermometer (Torabi and Pirnia, 2008). Lower temperatures are obtained with geothermometres based on Fe-Mg exchanges between olivine and spinel, reflecting sub-solidus re-equilibration (Irvine, 1967). This may affect the liquid composition calculated for the parental melt of the patchy chromitite, but not the massive lenses of Cr-spinels (e.g., Melcher et al., 1997). Such calculations have previously been applied to Oman, MOF massif BAT, Nan Uttaradit chromitites (Orberger et al., 1995) and layered Intrusions of Bushveld, Great Dyke and basalts of Barberton. The results are compared in Table 3. The liquids forming massive Cr-spinel of MOF contained 9-10wt% Al_2O_3 and had very low FeO/MgO ratios, around 0.3-0.5. The parental melts of the Oman chromitite had higher Al_2O_3 (> 11.4wt%) and MgO/FeO (average 0.62). In summary, the calculated amount of Al_2O_3 and FeO/MgO ratios in the parental melts of these examples, indicate a probable boninitic magma. On the other hand, high-Al spinel in the BAT chromitite may have equilibrated with liquids containing 13.5-16.7wt% Al_2O_3 and with FeO/MgO values of 0.8-1.0, which show MORB-type liquids for the parental melt. The composition of the parental melt of the Nain chromitite patches and lenses is similar to boninitic melts (e.g., Oman chromitites).

Boninite magmas are Si-rich, thus promoting Cr-spinel precipitation as a result of polymerization of the melt (Peck and Keays, 1990). Also, in contrast to MORB, boninite magmas are possibly derived from highly depleted mantle (Agata, 1988; Jan and Windley, 1990) and formed at the first stages of an island arc evolution (Middlemost, 1985).

Tectonic setting

Bonatti and Michael (1989) stated that the spinel composition of mantle peridotites depends on the geodynamic environment. The Cr# in spinel is a good indicator of the tectonomagmatic history of the host rock (e.g., Hajialioghli et al., 2007). Based on chemical data presented in this paper and in Ghazi et al. (2010b), the Cr-spinels in the lherzolites and harzburgites of the Nain ophiolites display low Cr# (< 60); such spinels normally are found in a mid-ocean ridge environment (including back-arc basins; Dick and Bullen, 1984). The Cr-spinels in chromitite patches and dunites display a range of Cr# (< 60 to > 60); such spinels may occur, for example, in areas where a young island arc is built on older oceanic crust (e.g., Miyashiro, 1973), or across the transitions from arc to oceanic lithosphere (Menzies et al., 1980), including back-arc basins (Arif and Jan, 2006). The Cr-spinels in chromitite lenses display a high Cr# (>, 60), similar to most island arc type complexes.

The boninitic magma-materials within the mantle sequence suggest that the Nain ophiolitic complex originated in a suprasubduction zone (SSZ) setting (e.g., Suhr and Edwards, 2000). It is commonly assumed that boninites are generated from strongly refractory mantle as a second stage melt, metasomatised by Ba and Sr-rich hydrous fluids released from the subducting slab (e.g., Orberger et al., 1995).

Canil (2004) infers that highly variable contents of Al_2O_3 are characteristic of orogenic peridotites. Since H-MRREs are incompatible elements and secondary processes such as alteration do not affect them, these elements can show the nature of the source materials. Metasomatism by fluids derived from the subducting slab can change the concentration of LREEs and LILEs to some extent. The positive anomalies of these elements are more evident in magmas generated in fore-arc basins and in rocks formed at the initiation of subduction. Chondrite-normalized REE patterns for these peridotites are clearly distinctive from the Wuqbah Central zone (Oman ophiolites) and Maqsad diapir, but are similar to abyssal peridotites such as Alpine peridotites and EPR (East Pacific Rise) peridotites that generated at the mid-ocean ridge (Fig. 12). Therefore, all the collected data on

Table 4 - Al_2O_3 (wt %) content and FeO/MgO ratios of the parental melt and calculated degree of partial melting (F).

	Chromitite patches			Chromitie lenses		Host rocks	
	Chromitite1	Chromitite2	Chromitite3	Chromitite (HA1)	Chromitite (HA2)	harzburgite	dunite
Al_2O_3 wt% spinel	20.33	21.37	20.31	13.78	14.87	32.84	26.91
Al_2O_3 wt% melt	13.59	13.87	13.58	11.58	11.95	16.77	15.58
FeO/MgO melt	0.99	0.99	1.1	0.83	0.84	1.33	1.63
F %	19.2	18.91	19.2	20.72	20.52	15.1	16.5

the peridotites from the Nain ophiolites point to a tectonic setting similar to a mid-ocean ridge, or more likely to a well developed back-arc basin.

Petrogenesis

Above subduction zones, decompression-melting (Sisson and Bronto, 1998) is facilitated and amplified by the presence of H_2O derived from the subducting slab (e.g., Green and Falloon, 1998). The presence of H_2O has a critical influence on melting proportions and mechanisms, since it: (i) lowers the peridotite solidus and increases the degree of fusion at a given temperature; (ii) decreases the relative contributions of olivine and clinopyroxene to the melt, allowing clinopyroxene to persist in the residua to higher degrees of fusion, and increases the contribution of orthopyroxene and (iii) favours incongruent fusion of orthopyroxene, generating olivine+Cr-spinel (e.g., Page et al., 2008).

Three processes for the generation of mantle dunite and chromitite are suggested: (1) residual material from extreme partial melting; (2) cumulates in magmatic conduits; (3) formation by reactions involving assimilation of pyroxene (e.g., Page et al., 2008). The Cr# of Cr-spinels in peridotites is a good tool for defining the degree of depletion of a mantle source. It increases as the rate of partial melting increases (Dick and Bullen, 1984; Kamenetsky et al., 2001). The formula of Hellebrand et al. (2001) was used for estimating the degree of partial melting of the source materials:

$$F\% = 10 \ln (Cr\#_{spinel}) + 24$$

where F% is the degree of partial melting. Table 4 shows the calculated F% for chromitite, dunite and harzburgite source materials. These rocks show small differences in the degree of partial melting, ranging from ~ 15 to ~ 21%. Experimental data show that a fertile lherzolite source produces a residual harzburgite at about 20% melting, and residual dunite at about 50-60% melting (Bonatti and Michael, 1989; Kostopoulos, 1991). These calculations are inconsistent with a residual origin for the studied peridotites. In fact, their whole rock chemistry (REE patterns), shows a partial melting degree lower than 18% (Fig. 8). This confirms that both types of Nain chromitites are not residual.

The presence of chromitite and dunite lenses, ultramafic rocks cumulus, veins of orthopyroxenite in harzburgites, impregnated peridotites and evidence of melt/peridotite interaction all imply channelled circulation of magma in the Nain mantle. Also, the presence of podiform chromitite with nodular textures is consistent with open-channelled melt migration and cumulus forming processes (Leblanc and Nicolas, 1992). Considering the above evidences, it seems that a mixed open-channel cumulate/rock-reaction model can be used to explain the formation of the studied podiform chromitite in the Nain ophiolites.

Magmatic and geodynamic evolution

Studies on the geodynamic environment where the Iranian ophiolites formed, based on mantle rocks chemistry are scarce. Chemistry data on ophiolitic mantle rocks such as Khoy, Nehbandan, Nain and Kermanshah suggest MORB and intra-oceanic subduction basins settings (e.g., Allahyari et al., 2010; Ghazi et al., 2010a; 2010b; Saccani et al., 2010). The study by Saccani et al. (2010) on the evolution of the mantle sequence of the Nehbandan ophiolites is very detailed and comprehensive. Thus, a comparison of the mantle rocks from Nain with those from the Nehbandan

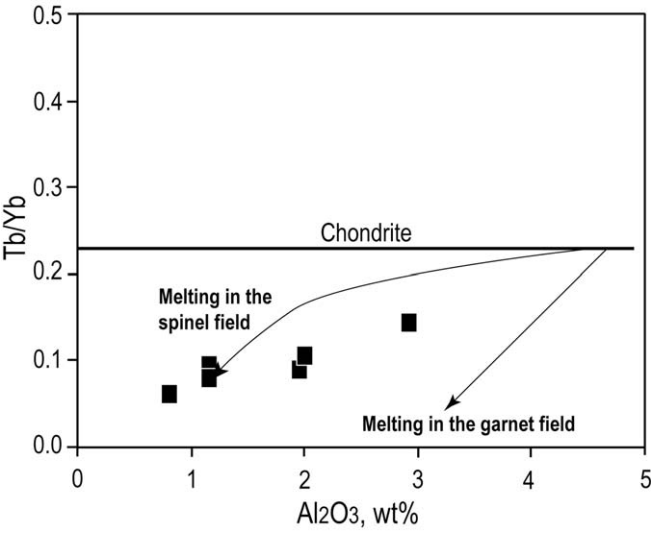

Fig. 10 - Al_2O_3 versus Tb/Yb diagram for peridotites of the Nain ophiolite. According to the diagram, melting of the source materials occurred in the spinel field within the mantle.

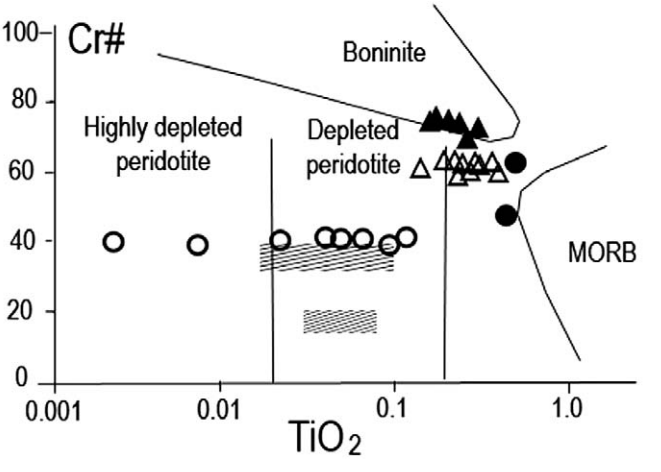

Fig. 11 - TiO_2 (wt%) versus Cr# of the studied Cr-spinels. See text for more explanations. Symbols are as in Fig. 9.

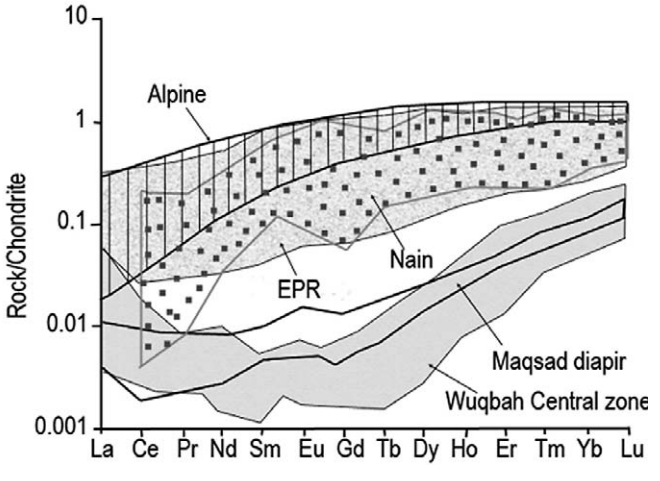

Fig. 12 - REE patterns of the Nain peridotites compared to chondrite-normalized REE patterns of the Wuqbah peridotites (Girardeau et al. 2002), Maqsad diapir peridotites (Godard et al., 2000), EPR peridotites (Niu and Hekinian, 1997), and Alpine peridotites (Li, 1992).

ophiolites, both bounding the CIM, seems to be suitable to provide valuable insights for a geodynamic reconstruction. Saccani et al. (2010) stated the presence of an oceanic basin between CIM and the Afghan blocks of mainly MORB type during the Jurassic. An intra-oceanic subduction during the Cretaceous was responsible for the genesis of subduction related rocks. Unlike the Nehbandan ophiolites, the Nain ophiolites are located between the Sanandaj-Sirjan Zone (active continental margin) and the CIM block. The evolution of this basin was driven by subduction of the Neotethys oceanic crust beneath the Sanandaj-Sirjan Zone.

After subduction inception of the Neo-Tethys oceanic lithosphere beneath the southern margin of the Central Iranian block (Sanandaj-Sirjan active zone), a back-arc basin developed between Sanandaj-Sirjan active zone and CIM during the Jurassic. Based on geochemical characters of the Nain rocks (Hassanipak and Ghazi, 2000), an intra-oceanic arc is supposed to be generated in this basin during Late Jurassic to Early Cretaceous. The lithospheric mantle wedge that supplied material for the arc magmas, become much depleted. Chromitite lenses, dunite and ultramafic cumulates were generated in this depleted lithospheric mantle.

A change in subduction regime in mid Cretaceous (e.g., Agard et al. 2006), caused the spreading of an oceanic back-arc basin in the Nain basin. Back-arc basin magmas were generated by decompression melting of the asthenospheric mantle under a spreading ridge in the same way like true MORB (e.g., Xu et al., 2003). During the formation of this back-arc basin, chromitite patches were generated. Therefore, chromitite lenses, dunite and ultramafic cumulates are the remnants of the Nain Ocean in the site of the arc suture with highly depleted lithospheric mantle, now recognized in the ophiolites as serpentinized rocks. Whole-rock and Cr-spinel chemistry of these peridotites and chromitite patches show that they probably formed in the mentioned oceanic back-arc basin, with the same characters found in mid-ocean ridge settings. Increments of mantle partial melts from MOR were possibly incomplete in the very incipient mid-ocean ridge as in the short-lived Nain back-arc basin (Pirnia et al., 2010). A simplified magmatic and geodynamic reconstruction of the Nain basin in the Cretaceous is shown in Fig. 13.

CONCLUSIONS

Chromitites in the Nain ophiolites occur as podiform bodies formed in the mantle. Based on field and petrographic observations and chemical characters of Cr-spinels, two types of chromitites have been recognized, occurring, respectively, as lenses and patches.

The boninitic parental melt composition and high Cr# of Cr-spinels of chromitite lenses indicate that they formed in an arc setting, while the geochemical characters of chromitite patches and peridotites of this ophiolites show that they generated in an oceanic back-arc basin. In this picture, the chromitite lenses and the host dunites, which are more depleted in comparison with chromitite patches and their host harzburgites, can be attributed to a depleted mantle wedge on the subduction zone.

In contrast, chromitite patches and their host harzburgites can be related to a more enriched mantle in the spreading site of a rather deep marginal basin, associated with a mantle plume.

It seems that a mixed open-channel cumulate/rock-reaction model is most compatible with our data and observations for explaining the formation of the Nain podiform chromitites. The mixed open-channel cumulate/rock-reaction system suggested here, could have been very active at the arc and during the early stages of rifting of a depleted mantle wedge. Therefore the formation of the chromitite lenses can be related to the arc system generating ascending melts, in which the Cr-spinels formed and show characteristics of boninitic spinels. In contrast, chromitite lenses, where the host rock Cr-spinels show intermediate characteristics of SSZ to MOR spinels, should have formed at the early stages of rifting.

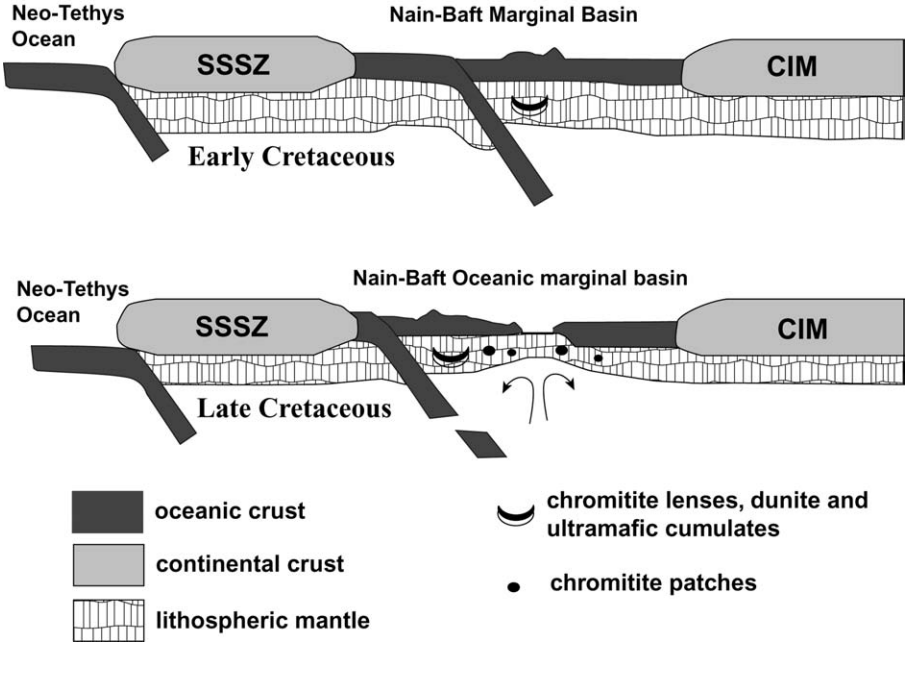

Fig. 13 - Highly schematized geodynamic and magmatic scenario for the evolution of the Nain oceanic basin in the Cretaceous. SSSZ: South Sanandaj-Sirjan Zone, CIM: Central Iranian micro-continent.

ACKNOWLEDGEMENTS

This work is part of the M.Sci. dissertation of the first author, which is supported financially by the Shahid Beheshti University of Tehran. We thank J. Ravaux from Université Nancy I for assistance in microprobe analyses. We also thank Dr. Emilio Saccani from Università di Ferrara for his invaluable help and for driving our attention to the existence of ultramafic cumulates in the Nain ophiolites. We are indebted to Prof. Michele Marroni for his help and efficient editorial handling of the paper. Deep gratitude is also owed to the anonymous reviewers of the journal for their constructive criticism.

REFERENCES

Agard P., Monie P., Gerber W., Omrani J., Molinaro M., Meyer B., Labrousse L.,Vrielynck B., Jolivet L. and Yamato P., 2006. Transient, synobduction exhumation of Zagros blueschists inferred from P-T, deformation, time, and kinematic constraints: Implications for Neotethyan wedge dynamics. Geophys. Res., 111: B11401, doi:10.1029/2005JB004103.

Agata T., 1988. Chrome spinels from the Oura layered igneous complex, central Japan. Lithos, 21: 97-108.

Allahyari K., Saccani E., Pourmoafi M., Beccaluva L. and Masoudi F., 2010. Petrology of mantle peridotites and intrusive mafic rocks from the Kermanshah ophiolitic complex (Zagros belt, Iran): implications fro the geodynamic evolution of the neo-Tethyan oceanic branch between Arabia and Iran. Ofioliti, 35 (2): 71-90.

Arai S., 1992. Chemistry of chromian spinel in volcanic rocks as a potential guide to magma chemistry. Mineral. Mag., 56: 173-184.

Arif M. and Jan M.Q., 2006. Petrotectonic significance of the chemistry of chromite in the ultramafic-mafic complexes of Pakistan J. Asian Earth Sci.; 27: 628-646.

Auge T., 1987. Chromite deposits in the northern Oman Ophiolite: mineralogical constraints. Mineral. Depos., 22: 1-10.

Berberian M. and King G.C.P., 1981. Towards a paleogeography and tectonic evolution of Iran. Can. J. Earth Sci., 18: 210-265.

Bonatti E. and Michael P.J., 1989. Mantle peridotites from continental rifts to ocean basins to subduction zones. Earth Planet. Sci. Lett., 91: 297-311.

Bonavia F.F., Diella V. and Ferrario A., 1993. Precambrian podiform chromitites from Kenticha Hill, Southern Ethiopia. Econ. Geol., 88: 198-202.

Canil D., 2004. Mildly incompatible elements in peridotites and the origins of mantle lithosphere. Lithos, 77: 375-393.

Casey. J., 1997. Comparison of major-and trace-element geochemistry of abyssal peridotites and mafic plutonic rocks with basalts from the Mark Region of Mid-Atlantic Ridge. Proc. ODP. Sci. Res., 153: 181-241.

Choi S.H., Shervais J.W. and Mukasa S.B., 2008. Suprasubduction and abyssal mantle peridotites of the Coast Range ophiolite, California. Contrib. Mineral. Petrol, 156: 551-576.

Conrad W.K. and Kay R.W., 1984. Ultramafic and mafic inclusions from Adak Island: crystallization history and implications for the nature of primary magmas and crustal evolution in the Aleutian arc. J. Petrol., 25: 88-125.

Davoudzadeh M., 1972. Geology and petrology of the area North of Nain, Central Iran. Geol. Surv. Iran. Rep., 1.

Desmons J. and Beccaluva L., 1983. Mid-oceanic ridge and island arc affinities in ophiolites from Iran: paleogeographic implication. Chem. Geol., 39: 39-63.

Dick H.J.B. and Bullen T., 1984. Chromian spinel as a petrogenetic indicator in abyssal and alpine-type peridotites and spatially associated lavas. Contrib. Mineral. Petrol., 86: 54-76.

Dick H.J.B. and Kelemen P.B., 1991. Chromian spinel as a petrogenetic indicator of magma genesis in shallow mantle rocks. EOS, 72: 142.

Emami M.H., Sadegi M.M. and Omrani S.J., 1993. Magmatic map of Iran. Scale 1:100000, Geol. Surv. Iran.

Ghasemi A. and Talbot C.J., 2006. A new tectonic scenario for the Sanandaj-Sirjan Zone (Iran) J. Asian Earth Sci., 26: 683-693.

Ghazi A.M., Hassanipak A.A., Mahoney J.J. and Duncan R.A., 2004. Geochemical characteristics, ^{40}Ar-^{39}Ar ages and original tectonic setting of the Band-e-Zeyarat/Dar Anar ophiolite, Makran accretionary prism, S. E. Iran. In: M. Flower (Ed.), Tectonophysics, 393: 175-196.

Ghazi J.M., Rahgoshay M., Shafaii Moghadam H. and Moazzen M., 2010a. Geochemistry of gabbroic pockets of a mantle sequence in the Nain ophiolite (Central Iran): Constraints on petrogenesis and tectonic setting of the ophiolite. N. Jb. Mineral. Abh., 187 (1): 49-62.

Ghazi J.M., Moazzen M., Rahgoshay M. and Shafaii Moghadam H., 2010b. Mineral chemical composition and geodynamic significance of peridotites from Nain ophiolite, central Iran. J. Geodyn., 49: 261-270.

Girardeau J., Monnier C., Lemee L. and Quatrevaux F., 2002. The Wuqbah peridotite, central Oman Ophiolite: Petrological characteristics of the mantle in a fossil overlapping ridge setting. Marine Geophy. Res., 23: 43-56.

Godard M., Jousselin D. and Bodinier J.L., 2000. Relationships between geochemistry and structure beneath paleo-spreading centre: a study of the mantle section in the Oman Ophiolite. Earth Planet. Sci. Lett.; 180: 133-148.

Green T.H. and Falloon T.J., 1998. Pyrolite: a Ringwood concept and its current expression. In: I. Jackson (Ed.), Earth's mantle: Composition, structure, and evolution. Univ. Press, Cambridge, p. 311-378.

Haggerty S.E., 1988. Upper mantle opaque mineral stratigraphy and the genesis of metasomaties and alkali-rich melts. J. Geol. Soc. Australia, 14: 687-699.

Hajialioghli R., Moazzen M., Droop G.T.R., Oberhänsli R., Bousquet R., Jahangiri A. and Ziemann M., 2007. Serpentine polymorphs and P-T evolution of metaperidotites and serpentinites in the Takab area, NW Iran. Mineral. Mag., 71 (2): 203-222.

Hassanipak A.A. and Ghazi A.M., 2000. Petrochemistry, ^{40}Ar-^{39}Ar ages and tectonics of the Nain Ophiolite, Central Iran. GSA Annual Meeting, Reno, Nevada, p. 237-238.

Hellebrand E., Snow J.E., Dick H.J.B. and Hofmann A.W., 2001. Coupled major and trace elements as indicators of the extent of melting in mid-ocean ridge peridotites. Nature, 410 (6829): 677-681.

Hickey R.L. and Frey F.A., 1982. Geochemical characteristics of boninite series volcanics: implications for their source. Geochim. Cosmochim. Acta, 46: 2099-2115.

Irvine T.N., 1965. Chromian spinel as a petrogenetic indicator. Part I Theory. Can. J. Earth Sci., 2: 648-672.

Irvine T.N., 1967. Chromian spinel as a petrogenetic indicator, part 2. Petrologic applications. Can. J. Earth Sci., 4: 71-103.

Jakes P. and White A.J.R., 1972. Major and trace element abundances in volcanic rocks of orogenic areas. Geol. Soc. Am. Bull., 83: 29-40.

Jan M.Q. and Windley B.F., 1990. Chromian spinel-silicate chemistry in ultramafic rocks of the Jijal complex Northwestern Pakistan. J. Petrol., 34: 667-715.

Johan Z., Robert J.L. and Volfinger M., 1982. Role of reducing fluids in the origin of chromite deposits from ophiolitic complexes. Geol. Ass. Canada, Abstr., 7: 58.

Kamenetsky V., Crawford A.J. and Meffre S., 2001. Factors controlling chemistry of magmatic spinel: an empirical study of associated olivine, Cr-spinel and melt inclusions from primitive rocks. J. Petrol., 42: 655-671.

Kepezhinskas P.K., Defant M.J. and Drummond M.S., 1995. Na metasomatism in the island-arc mantle by slab melt-peridotite interaction: evidence from mantle xenoliths in the North Kamchatka arc. J. Petrol., 36: 1505-1527.

Kostopoulos D.K., 1991. Melting of shallow upper mantle: a new perspective. J. Petrol., 32: 671-699.

Lanphere M.A. and Pamić J., 1983. $^{40}Ar/^{39}Ar$ age and tectonic setting of ophiolites from Neyriz area, south-east Zagros ranges, Iran. Tectonophysics, 96: 245-256.

Leblanc M. and Nicolas A., 1992. Les chromitites ophiolitiques. Chron. Rech. Minière, 507: 3-25.

Li C.N., 1992. Petrology of igneous trace elements. China Univ. Geosci. Press, Wuhan (in Chinese).

Maurel C. and Maurel P., 1982. Étude expérimentale de la solubilité du chrome dans les bains silicatés basiques et sa distribution entre liquide et minéraux coexistants: conditions d'existence du spinelle chromifère. Bull. Minéral., 105: 640-647.

McCall G.J.H., 1997. The geotectonic history of the Makran and adjacent areas of southern Iran. J. Asian Earth Sci., 15: 517-531.

McDonough W.F. and Sun S.S., 1995. The composition of the Earth. Chem. Geol., 120: 223-253.

Medaris Jr. G., Wang H., Jelínek E., Mihaljevič M. and Jakeš P., 2005. Characteristics and origins of diverse Variscan peridotites in the Gföhl Nappe, Bohemian Massif, Czech Republic. Lithos, 82: 1-23

Melcher F., Grum W., Simon G., Thalhammer T.V. and Stumpfl E.F., 1997. Petrogenesis of the ophiolitic giant chromite deposits of Kempirsai, Kazakhstan: a study of solid and fluid inclusions in chromite. J. Petrol., 38: 1419-1458.

Melson W.G., Vallier T.L., Wright T.L., Byerly G. and Nelson J., 1976. Chemical diversity of abyssal volcanic glass erupted along Pacific, Atlantic and Indian Ocean sea-floor spreading centers. In: The geophysics of the Pacific Ocean basin and its margin. Am. Geophys. Union., p. 351-367

Menzies M., Blanchard D.P. and Xenophontos C., 1980. Genesis of the Somerville arc-ophiolite, Sierra Nevada foothills, California. In: A.J. Irving and M.A. Dungan (Eds.), The Jackson Volume. Am. J. Sci., 280-A: 329-344.

Mercier J.-C.C. and Nicolas A., 1975. Textures and fabrics of upper-mantle peridotites as illustrated by xenoliths from basalts. J. Petrol., 16: 454-487.

Meyer B., Mouthereau F., Lacombe O. and Agard P., 2006. Evidence of Quaternary activity along the Dehshir fault: implication for the Tertiary tectonics of Central Iran. Geophys. J. Int., 164: 192-201.

Middlemost E.A.K., 1985. An introduction to igneous petrology: Magma and magmatic rocks. Longman.

Miyashiro A., 1973. The Troodos ophiolitic complex was probably formed in an island arc. Earth Planet. Sci. Lett., 19: 218-224.

Moazzen M., Omrani H., Oberhänsli R., Moayyed M., Tsujimori T. and Bousquet R., 2010. Shanderman eclogites from Northern Iran; P-T path and Paleotethys geodynamics from subduction to exhumation. MSA Meeting, Tectonic Crossroads: Evolving Orogens of Eurasia-Africa-Arabia. Oct. 2010, Ankara.

Monnier C., Girardeau J., Maury R. and Cotten J., 1995. Back-arc basin origin for the East Sulawesi ophiolite (eastern Indonesia). Geology, 23: 851-854.

Niu Y., 1997. Mantle melting and melt extraction processes beneath ocean ridges: evidence from abyssal peridotites. J. Petrol., 38: 1047-1074.

Niu Y. and Hékinian R., 1997, Basaltic liquids and harzburgitic residues in the Garrett Transform: a case study at fast-spreading ridges. Earth Planet. Sci. Lett. 146: 243-258.

Orberger B., Lorandb J.P., Girardeau J., Mercier J-C.C. and Pitragool S.,1995. Petrogenesis of ultramafic rocks and associated chromitites in the Nan Uttaradit ophiolite, Northern Thailand. Lithos, 35: 153-182.

Pagé P., Jean H., Bédard J.H., Schroetter J.M. and Tremblay A., 2008. Mantle petrology and mineralogy of the Thetford Mines Ophiolite Complex. Lithos, 100: 255-292.

Peck D.C. and Keays R.R., 1990. Geology, geochemistry, and origin of platinum-group element-chromitite occurrences in the Heazlewood River Complex, Tasmania. Econ. Geol., 85: 765-793.

Pirnia T., Arai S. and Torabi G., 2010. Post-deformational impregnation of depleted MORB in Nain lherzolite (Central Iran). J. Mineral. Petrol. Sci., 105: 74-79.

Proenza J.A., Zaccarini F., Lewis J.F., Longo F. and Garuti G., 2007. Chromian spinel composition and the platinum-group minerals of the PGE-rich Lomapegvera chromitites, Loma Caribe peridotite, Donimican Republic. Can. Mineral., 45: 631-648.

Rahgoshay and Shaffaii Moghadam H., 2004. Metamorphism stages in Nain ophiolitic massif, Central Iran. 5th Intern. Symp. Eastern Mediterranean Geol, Greece, Proceed., p. 271-274.

Rahmani F., Noghreyan M. and Khalili M., 2007. Geochemistry of sheeted dikes in the Nain ophiolite (Central Iran). Ofioliti, 32 (2): 119-129.

Ruttner A.W., 1993. Southern borderland of Triassic Laurasia in north-east Iran. Geol. Runds., 82: 110-120.

Saccani E., Delavari M., Beccaluva L. and Amini S. 2010. Petrological and geochemical constraints on the origin of the Nehbandan ophiolitic complex (eastern Iran): Implication for the evolution of the Sistan Ocean. Lithos, 117: 209-228.

Schmit K. and Soffel H., 1983. Mesozoic-Cenozoic geological events in Central-East Iran and their relation to paleomagnetic results, In: Geodynamic Project (Geotraverse) in Iran. Geol. Surv. Iran, 55: 27-35.

Shafaii Moghadam H., Rahgoshay M., Whitechurch H. and Montigny R., 2007. A geochemical scenario for evolution of the Nain-Baft back-arc basin. Goldschmidt Conference Abstr., p. A920.

Sharpe M.R. and Hulbert L.J., 1985. Ultramafic sills beneath the Eastern Bushveld Complex: Mobilized suspensions of early Lower Zone cumulates in a parental magma with boninitic affinities. Econ. Geol., 80: 849-871.

Shirdashtzadeh N., Torabi G. and Arai S., 2010. Metamorphism and metasomatism in the Jurassic Nain ophiolitic mélange, Central Iran. N. Jb. Geol. Paläont. Abh., 255 (3): 255-275.

Shojaat B., Hassanipak A.A., Mobasher K. and Ghazi A.M., 2003. Petrology, geochemistry and tectonics of the Sabzevar ophiolite, North Central Iran. J. Asian Earth Sci., 21: 1053-1067.

Sisson T.W. and Bronto S., 1998. Evidence for pressure-release melting beneath magmatic arcs from basalt at Galunggung, Indonesia. Nature, 391: 883-886.

Snow J.E. and Dick H.J.B., 1995. Pervasive magnesium loss by marine weathering of peridotite. Geochim. Cosmochim. Acta, 59: 4219-4235.

Stöcklin J., 1974. Possible ancient continental margin in Iran. In: C.A. Burke and C.L. Drake (Eds.), The geology of continental margins. Springer, New York, p. 873-887.

Stowe C.W., 1994. Compositions and tectonic settings of chromite deposits through time. Econ. Geol., 89: 528-546.

Suhr G. and Edwards S.J., 2000. Contrasting mantle sequences exposed in the Lewis Hill massif: evidence for the early, arc-related history of the Bay of Islands ophiolite. In: Y. Dilek, E.M. Moores, D. Elthon and A. Nicolas (Eds.), Ophiolites and oceanic crust: New insights from field studies and the Oceanic Drilling Program. Geol. Soc. Am. Spec. Paper, 349: 433-442.

Sun S.S. and McDonough W.F., 1989. Chemical and isotopic systematics of oceanic basalts: implications for mantle composition and processes. In: A.D. Saunders and M.J. Norry (Eds.), Magmatism in the ocean basins. Geol. Soc. London Spec. Publ., 42: 313-345.

Sun S.S. and Nesbitt W., 1978. Geochemical regularities and genetic significance of ophiolitic basalts. Geology, 6: 689-693.

Takin M., 1972. Iranian geology and continental drift in the Middle East. Nature, 235: 147-150.

Torabi G. and Pirnia T., 2008. Petrology of mantle peridotites in Naein Ophiolitic Mélange. Iranian Res. J. Sci., Univ. Isfahan, 30 (1): 167-190.

Torabi G., Noorbehesht I., Shirdashtzadeh N. and Pirnia T., 2007. Geothermometry of skarns in the Nain ophiolitic mélange (Isfahan Province). Iranian J. Crystal. Mineral., 2: 357-382.

Wilson A.H., 1982. The geology of the Great 'Dyke', Zimbabwe: the ultramafic rocks. J. Petrol., 23: 240-292.

Xu X., O'Reilly S.Y., Griffin W.L. and Zhou X., 2003. Enrichment of upper mantle peridotite: petrological, trace element and isotopic evidence in xenoliths from SE China. Chem. Geol., 198: 163-188.

Received, February 2, 2011
Accepted, June 10, 2011